Statistics-tuned entanglement of the boundary modes in coupled Su-Schrieffer-Heeger chains

Saikat Santra,[*] Adhip Agarwala,[†] and Subhro Bhattacharjee[‡]
International Centre for Theoretical Sciences, Tata Institute of Fundamental Research, Bengaluru 560089, India

(Received 28 October 2020; revised 14 April 2021; accepted 15 April 2021; published 17 May 2021)

We show that mutual statistics between quantum particles can be tuned to generate emergent novel few-particle quantum mechanics for the boundary modes of symmetry-protected topological phases of matter. As a concrete setting, we study a system of pseudofermions, defined as quantum particles with tunable algebra, which lie on two distinct Su-Schrieffer-Heeger (SSH) chains. We find that as the mutual statistics of the particles are tuned—the boundary modes present in the two chains gets nontrivially entangled showing a sudden jump in their mutual entanglement entropy. We further show that such tuning of statistics engenders a first-order transition between two topologically nontrivial phases which differ in the behavior of interchain entanglement. Using a combination of analytical and numerical techniques and effective modeling, we uncover the rich physics that this system hosts. The results are of particular relevance in context of the study of the effective low-energy quantum mechanics of topological edge modes in one hand and their recent realization in ultracold atoms on the other. This then provides for controlled manipulation of such low-energy modes.

DOI: 10.1103/PhysRevB.103.195134

I. INTRODUCTION

Topological phases of matter show a multitude of exotic phenomena with crucial implications for the theoretical framework of understanding condensed matter phases on one hand, and material sciences with technological perspectives on the other [1–11]. Characteristically, several such systems specifically in one spatial dimension, hosts symmetry protected topological (SPT) boundary *zero* modes [12–14] as the manifestation of the nontrivial quantum entanglement in these systems. The low-energy physics of these systems are then governed effectively by the properties of the few boundary-modes.

This *emergent* few-particle quantum mechanics of the novel boundary modes is extremely rich and forms the essential ingredient for estimating the usefulness as candidates for material realization of quantum computing [14–20] where such boundary modes serve as *qubits* [21–23]. Theoretical studies examining such boundary modes in coupled-wire systems [24–28], their tunability in junctions [15,22,29] and attempts to entangle them nontrivially are been vigorously pursued in this regard [15,21,22,30–32]. The complementary issue at the experimental front of controlled manipulation and tuning of such boundary modes are also being currently explored in wide variety of different materials [16,33–41] as well as in cold atom systems [42–46].

It is crucial therefore to identify potential microscopic "knobs" that can be "tuned" to manipulate the low-energy physics of these topologically nontrivial boundary modes, and investigate their interplay with the symmetries. In addition to this tuning of few particle quantum mechanics, these knobs can further engineer novel phase transitions in the underlying many-body system.

In this paper, we investigate the above issues in context of the paradigmatic Su-Schrieffer-Heeger (SSH) model for polyacetylene [12,13] that stabilizes symmetry protected topological boundary modes. We examine an interesting tuning parameter that is of relevance in context of recent experimental [46,47] and theoretical [48–50] developments—the *generalized algebra* of the interacting fermions—and study it in context of two coupled SSH chains as shown in Fig. 1. The *statistical* tuning parameter, ϕ [see Eq. (1)], allows the degrees of freedom to smoothly transform from being fermionic to (hard core) bosonic and vice-versa in one spatial dimension. Such degrees of freedom, referred as *pseudofermions* [50], are generalizations of "anyons" in one dimension [48,51–73]. Quite remarkably, this anyonic physics has been recently realized experimentally in a cold atomic setting [47].

In our system, we find that as $\phi \in [0, \pi]$ is tuned, two topologically nontrivial SSH chains get mutually entangled. In particular, we uncover the rich low-energy physics of the many-body boundary modes of a finite, but long, system—as is relevant for the experiments. Crucially, ϕ allows modulation of the entanglement properties of the boundary modes residing on the two chains. The bulk, in the mean time, undergoes a first-order transition at $\phi = \pi/2$, between the two topologically nontrivial phases. We use a combination of numerical techniques [exact diagonalization (ED), density-matrix renormalization group (DMRG)] and analytical methods to uncover the physics of this system with particular emphasis to the emergent quantum mechanics of the boundary modes.

The rest of this work is organized as follows. In Sec. II, we introduce the model and discuss its various relevant symmetries. In Sec. III, we discuss how this system stabilizes many-body boundary modes and study its dispersion as a function of ϕ. In Sec. IV, we develop an effective theory

[*]saikat.santra@icts.res.in
[†]adhip.agarwala@icts.res.in
[‡]subhro@icts.res.in

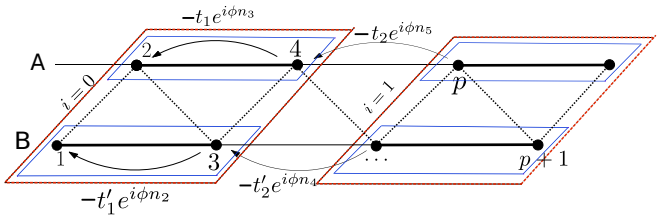

FIG. 1. Model. Schematic figure showing two SSH chains (A and B) labeled by site indices p. i labels the four site unit cell where t_1 and t_1' (t_2 and t_2') are the intra (inter) unit cell hopping strengths as shown. Every hopping term has an additional phase ϕ that depends on the fermionic occupation of an intermediate site lying on the other chain—this implements the pseudofermionic statistics (see text).

for these boundary modes; in particular, we study the case when both the chains contain one pseudofermion each and investigate how the boundary modes belonging to two chains get nontrivially entangled showing a sudden jump in mutual entanglement. We further develop an understanding of this physics using few-particle quantum mechanics of effective boundary modes. We further examine the stability of these boundary modes to disorder and symmetry breaking perturbations. In Sec. V, we begin investigating the half-filled many-body system. Here we find that, while ϕ keeps the system topologically nontrivial—there are in fact two distinctive phases at $\phi = 0$ and $\phi = \pi$, which are separated by a first-order phase transition. Using many-body trial wave functions, we identify the nature of the many-body ground states and further discuss the role of symmetry breaking perturbations on this many-body system. In Sec. VI, we summarize our results and provide concluding comments. In Appendices, we present additional results on DMRG calculations and role of disorder in these systems.

II. SSH MODEL FOR PSEUDOFERMIONS

We start by introducing the *pseudofermions* [50] and their generalized algebra. Consider a two dimensional local Hilbert space at each site p of a one dimensional lattice that are created and annihilated by second quantized *pseudofermions* operators $a_p^\dagger$ and a_p respectively with $N_p = a_p^\dagger a_p$ being the number operator. The generalized algebra is now given by

$$\begin{aligned} a_q a_p + a_p a_q e^{\mathrm{i}\phi\ \mathrm{sign}(p-q)} &= 0, \\ a_q a_p^\dagger + a_p^\dagger a_q e^{-\mathrm{i}\phi\ \mathrm{sign}(p-q)} &= \delta_{pq}, \end{aligned} \tag{1}$$

where $\mathrm{sign}(0) = 0$ gives an onsite fermionic algebra. The off-site algebra can be tuned from fermionic to (hard core) bosonic by tuning *statistical parameter* $\phi \in [0, \pi]$. Particles satisfying the above algebra have been previously dubbed as pseudofermions [50]—a nomenclature that we continue to use in the present work.

We take two decoupled SSH chains of pseudofermions given by the Hamiltonian

$$\begin{aligned} H = &- \sum_{i=0}^{L-1} [t_1 a_{4i+2}^\dagger a_{4i+4} + t_2 a_{4i+4}^\dagger a_{4i+6} + \mathrm{H.c.}] \\ &- \sum_{i=0}^{L-1} [t_1' a_{4i+1}^\dagger a_{4i+3} + t_2' a_{4i+3}^\dagger a_{4i+5} + \mathrm{H.c.}], \end{aligned} \tag{2}$$

where $i = 0, \ldots, L-1$ sums over L unit cells of four site each such that total number of sites (labeled by $p = 1, \ldots, N$) $N = 4L$ (see Fig. 1). $t_1(t_1')$ and $t_2(t_2')$ are the hopping amplitudes on the odd and even bonds of the upper A (lower B) chain. We can consider all these parameters to be distinct, however we will restrict them shortly.

The $\phi = 0$ limit clearly gives two decoupled free fermion chains whose properties are well known from the seminal works starting with those of Su, Schrieffer, and Heeger [12]. Here we summarize the relevant part of these results for completeness. Choosing a two site unit cell for each of the chains separately (see Fig. 1) the Hamiltonian for chain A (even indexed sites) and B (odd indexed sites) can be straightforwardly diagonalized to obtain the single-particle spectra for periodic boundary conditions:

$$E_A(k) = \pm\sqrt{(t_1 + t_2\cos(k))^2 + (t_2\sin(k))^2}, \tag{3}$$

$$E_B(k) = \pm\sqrt{(t_1' + t_2'\cos(k))^2 + (t_2'\sin(k))^2} \tag{4}$$

with $k \in [-\pi, \pi]$. At half-filling, this system is gapped at all values of t_1, t_2, t_1' and t_2', except when $t_1 = t_2 (t_1' = t_2')$. In the gapped phase, the ground state hosts a topological band with a nontrivial winding number when $t_1 < t_2 (t_1' < t_2')$ [74]. In such a topological phase, each individual chain under open boundary conditions, where the couplings between the $i = (L-1)$-th unit cell and $i = 0$-th unit cell are removed, can host two *degenerate* single-particle boundary modes which are localized at the two ends of the open chain.

The localization length of these boundary modes depends on the bulk gap and is given by $\zeta = 1/\ln\frac{t_2}{t_1}$ on chain A and similarly $\zeta' = 1/\ln\frac{t_2'}{t_1'}$ on chain B. In any finite sized system, these localized states however hybridize leading to bonding and antibonding orbitals, exponentially close in energy by a gap scale $\sim \exp(-L/\zeta)$ and $\sim \exp(-L/\zeta')$ for chains A and B, respectively. At this point we find it convenient to restrict parameter space by choosing $t_1' = \gamma t_1$ and $t_2' = \gamma t_2$ where we take $\gamma = 2$ unless otherwise stated. This particular parametrization proves helpful for energetic reasons as discussed below and does not affect the generality of our results. Importantly, given the recent realization of the SSH model in ultracold atoms [46], such a parametrization opens up ways for controlled manipulation of the boundary modes.

Finite ϕ poses an interacting problem, and this becomes explicit, following Ref. [50], once we recast Eq. (2) in terms of spinless fermions created and annihilated by $c_p^\dagger$ and c_p respectively through a fractional Jordan-Wigner transformations:

$$c_p = K_p a_p, \quad c_p^\dagger = a_p^\dagger K_p^\dagger \ \text{ with } \ K_p = e^{-\mathrm{i}\phi\sum_{q<p} n_q}. \tag{5}$$

whence the Hamiltonian in Eq. (2) becomes

$$H = H_A + H_B, \tag{6}$$

where H_A describes the hoppings on chain A, which now has ϕ dependent terms that depend on the site occupancies of chain B, i.e.,

$$H_A = -\sum_{i=0}^{L-1} [t_1 e^{\mathrm{i}\phi n_{4i+3}} c_{4i+2}^\dagger c_{4i+4} + \mathrm{H.c.}]$$

$$-\sum_{i=0}^{L-1}[t_2 e^{\mathbb{i}\phi n_{4i+5}} c^\dagger_{4i+4} c_{4i+6} + \text{H.c.}], \tag{7}$$

and similarly H_B describes the hoppings on chain B with ϕ dependent terms that depend on the site occupancies of chain A, i.e.,

$$H_B = -\sum_{i=0}^{L-1}[t_1' e^{\mathbb{i}\phi n_{4i+2}} c^\dagger_{4i+1} c_{4i+3} + \text{H.c.}] - \sum_{i=0}^{L-1}[t_2' e^{\mathbb{i}\phi n_{4i+4}} c^\dagger_{4i+3} c_{4i+5} + \text{H.c.}]. \tag{8}$$

Here, c_p now obeys usual fermionic anticommutation algebra. At any ϕ, the number density $n_p = c_p^\dagger c_p = N_p$ and hence the filling remains unchanged under the transformation [Eq. (5)].

Given the nonlocal character of the transformation, the description of phases and their transitions depend on the choice of underlying microscopic degrees of freedom. For instance the standard Jordan-Wigner transformation can take the symmetry-broken ground states of the transverse field Ising model to the symmetry-protected topological states of the Majoranas [14]. The same transformation on the SSH model of fermions however takes fermionic SPT states to ground states of XY dimerized magnet which retains the SPT order albeit by a different representation [46]. In our paper, for having a consistent description of the phases and their transitions we discuss the physics in terms of the underlying c fermions.

A distinct feature of Eq. (2) and hence Eq. (6) is the fact that the total number of particles in each chain A and B remain independently conserved leading to a $U_A(1) \times U_B(1)$ symmetry for the system. This is in spite of the interaction between the c fermions of the two chains mediated by $\phi \neq 0$ through the physics of correlated hopping [50]. This is reminiscent of the coulomb drag in bilayer systems [75–77].

Continuing with the symmetries of the system, a single SSH chain made of $2L$ sites [46] say of the form

$$H_S = -\sum_{i=0}^{L-1}[t_1 c^\dagger_{2i+1} c_{2i+2} + t_2 c^\dagger_{2i+2} c_{2i+3} + \text{H.c.}] \tag{9}$$

is symmetric under staggered charge conjugation operation implemented by an antiunitary operator

$$\mathcal{C} = \left[\prod_i (c^\dagger_{2i+1} + c_{2i+1})(c^\dagger_{2i+2} - c_{2i+2})\right] \circ \boldsymbol{K} \tag{10}$$

(where $\boldsymbol{K}$ is the complex conjugation operator) such that

$$\mathcal{C} c_p \mathcal{C}^{-1} \to \begin{cases} c_p^\dagger & \forall\ p \in \text{odd} \\ -c_p^\dagger & \forall\ p \in \text{even} \end{cases}. \tag{11}$$

This can be generalized for the present case for the two chains and arbitrary ϕ by defining

$$U_o = \left[\prod_i (c^\dagger_{4i+1} + c_{4i+1})(c^\dagger_{4i+3} - c_{4i+3})\right]\left[\prod_i e^{-\mathbb{i}\frac{\phi}{2}\{(4i+2)n_{4i+2} + (4i+4)n_{4i+4}\}}\right] \circ \boldsymbol{K}, \tag{12}$$

$$U_e = \left[\prod_i (c^\dagger_{4i+2} + c_{4i+2})\left(c^\dagger_{4i+4} - c_{4i+4}\right)\right]\left[\prod_i e^{-\mathbb{i}\frac{\phi}{2}\{(4i+1)n_{4i+1} + (4i+3)n_{4i+3}\}}\right] \circ \boldsymbol{K} \tag{13}$$

such that

$$U_o c_{4i+a} U_o^{-1} \to \begin{cases} c^\dagger_{4i+1} & \forall\ i \text{ and } a = 1 \\ e^{\mathbb{i}\frac{\phi}{2}(4i+2)} c_{4i+2} & \forall\ i \text{ and } a = 2 \\ -c^\dagger_{4i+3} & \forall\ i \text{ and } a = 3 \\ e^{\mathbb{i}\frac{\phi}{2}(4i+4)} c_{4i+4} & \forall\ i \text{ and } a = 4 \end{cases} \tag{14}$$

and

$$U_e c_{4i+a} U_e^{-1} \to \begin{cases} e^{\mathbb{i}\frac{\phi}{2}(4i+1)} c_{4i+1} & \forall\ i \text{ and } a = 1 \\ c^\dagger_{4i+2} & \forall\ i \text{ and } a = 2 \\ e^{\mathbb{i}\frac{\phi}{2}(4i+3)} c_{4i+3} & \forall\ i \text{ and } a = 3 \\ -c^\dagger_{4i+4} & \forall\ i \text{ and } a = 4 \end{cases}. \tag{15}$$

Note that while $U_o(U_e)$ leads to staggered charge conjugation in the odd B (even A) chain, it leads to a multiplication by a site dependent phase in the even A (odd B) chain. Further, both U_e and U_o reduces to $\mathcal{C}$ operators for the respective chains A and B when $\phi = 0$. Among other symmetries, it is useful to note that presence of nonzero ϕ breaks the time-reversal symmetry in the system. Also, the spectrum at any ϕ is symmetric about zero energy—this is due to the bipartite structure of the Hamiltonian Eq. (6). A unitary symmetry operation of the form $c^\dagger_{4i+a} \to c^\dagger_{4i+a} (a = 1, 2)$, $c^\dagger_{4i+a} \to -c^\dagger_{4i+a} (a = 3, 4)$ takes $H \to -H$ and guarantees that E and $-E$ states occur in pairs. At $\phi = 0$, the boundary modes of each of the SSH chains are protected by $\mathcal{C}$ leading to a total of four localized edge modes. We now discuss the fate of the system at finite ϕ which, as we shall show, leads to nontrivial entanglement of the boundary modes of the two chains.

III. INTERACTIONS AND MANY-BODY BOUNDARY MODES

Absence of time-reversal and presence of $U_o U_e$ places our system in class D of the Altland-Zirnbauer [2,78,79] classification. However, for general $\phi \neq 0$, the system is interacting and does not necessarily belong to one of the ten classes of free fermion SPTs [80,81]. Here we are mainly interested in the fate of the boundary modes of a finite but long system at general values of ϕ. This allows us to engineer protocols for manipulating their properties using ϕ as a tuning parameter interpolating between the two limits of free fermions and hard-core bosons. Therefore we immediately focus on these

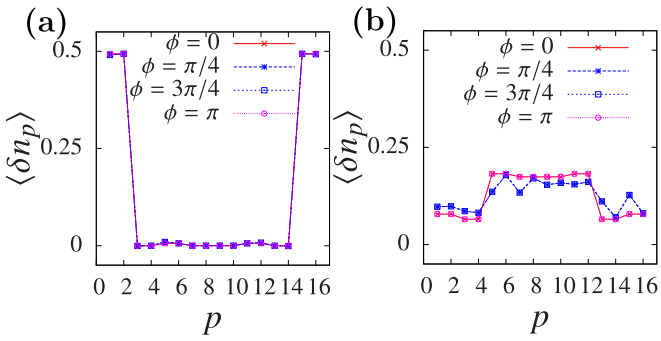

FIG. 2. Boundary density. Difference of particle densities ($\langle \delta n_p \rangle$) between the ground states for $\tilde{N}_{pf} = 2L$ and $\tilde{N}_{pf} = 2L - 2$ particle number sector, as a function of sites p for various values of ϕ in (a) the topological regime ($t_1 = 0.1 = 1 - t_2$) and (b) the trivial regime ($t_1 = 0.9 = 1 - t_2$). In (a), the values are normalized over all the four quasidegenerate ground states for $\tilde{N}_{pf} = 2L$ sector (see text) (ED, $\gamma = 2$, and $N = 16 = 4L$).

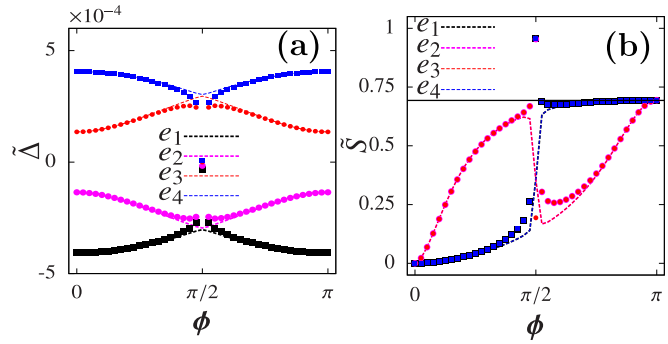

FIG. 3. Many body boundary excitations. (a) Energy of the four boundary modes for a half-filled system with open boundary conditions as measured by the *two-particle* gap defined by Eq. (16) (shown using points). (b) The corresponding mutual entanglement between the chains A and B with bulk contribution removed [see Eq. (17)] (shown using points) saturates to a value of ln(2) (shown by a solid line) (ED, $N = 4L = 16, t_1 = 0.1, t_2 = 1 - t_1, \gamma = 2$). Dashed lines ($e_1 \ldots e_4$) represent the results from two-particle problem as discussed in Sec. IV. The erratic behavior of energies and entanglement entropy exactly at $\phi = \frac{\pi}{2}$ [in both (a) and (b)] is due to a bulk transition which we discuss in Sec. V.

boundary modes while the complete characterization of the bulk physics is deferred to Sec. V.

In the topological phase ($t_1 < t_2, \phi = 0$), a half-filled open system should comprise of many-body boundary modes at low energies. To estimate the number of such states it is worthwhile to note that the free fermionic limit ($\phi = 0$) hosts four single-particle boundary modes close to zero energy which reside on the boundary while all other states ($4L - 4$) reside in the bulk. Therefore, in a system with number of fermions $= 2L - 2$ ($L - 1$ on each chain), only the single-particle bulk states would get occupied with no contribution from the boundary modes, generating a unique ground state. However, in a half-filled system, i.e., with number of fermions ($=2L$), two particles now occupy the single-particle boundary modes. The latter can be achieved in four ways while maintaining the condition that each chain has one boundary mode occupied. These thus correspond to *four* many-body quasidegenerate ground states for a half-filled system at $\phi = 0$ and $t_1 < t_2$ with open boundary conditions. When $t_1 > t_2$ (i.e., in the trivial regime) we have a unique ground state for both $2L - 2$ and $2L$ fermion number sectors, given the absence of any boundary modes.

The discussion above shows that for $t_1 < t_2$ a difference in particle densities at any site between the (four) ground states for $2L$ particles and the ground state for $2L - 2$ particles should reveal the boundary character of the many-body wave functions at half-filling, if any. In contrast, for trivial phase ($t_1 > t_2, \phi = 0$) given the absence of any single-particle boundary modes, one expects such a density difference between the two ground states at $2L$ and $2L - 2$ particle sectors would not have any specific boundary character. Extending this understanding at $\phi \neq 0$, we calculate the difference in particle densities at every site for number of pseudofermions, $\tilde{N}_{pf} = 2L$ system (averaged over the four lowest energy states for $t_1 < t_2$ and unique state for $t_1 > t_2$) and for $\tilde{N}_{pf} = 2L - 2$ system. We find that even when $\phi \neq 0$ and $t_1 < t_2$ (topological phase) the residual densities (normalized over all the four degenerate states) are $\sim$0.5 on the boundary sites [see Fig. 2(a)]; however, when $t_1 > t_2$ (trivial phase) the residual densities lie in the bulk showing that the system with $\tilde{N}_{pf} = 2L - 2$ should be considered as two delocalized holes which distribute uniformly over the bulk sites [see Fig. 2(b)]. This shows that the boundary modes remain intact for the entire parameter regime of $\phi \in [0, \pi]$ and thereby continuously interpolating between the "fermionic" ($\phi = 0$) and the (hard core) "bosonic" ($\phi = \pi$) limits.

Given the existence of such boundary modes for $t_1 < t_2$ and $\phi \neq 0$, we track the energetics of the quasidegenerate subspace by calculating the symmetrized *two-particle* gap given by

$$\tilde{\Delta} = E(\tilde{N}_{pf} = 2L) - \tfrac{1}{2}(E(\tilde{N}_{pf} = 2L + 2) + E(\tilde{N}_{pf} = 2L - 2)), \quad (16)$$

where E is the ground-state energy for $\tilde{N}_{pf}$ pseudofermions in a system of L unit cells with open boundary conditions. As defined, $\tilde{\Delta}$ measures the energy cost to populate the boundary modes of our system in the topological phase [see Eq. (16)] at a given value of ϕ. The resulting behavior of $\tilde{\Delta}$ is shown in Fig. 3(a). The figure also shows that the modulation of energy of the boundary modes occurs at a much smaller scale compared to the single-particle bulk gap [see Fig. 10(d)] and hence proving that the boundary modes retain their sanctity for all ϕ except at $\phi = \frac{\pi}{2}$.

To further probe the nature of the four energetically isolated (from the bulk) boundary modes at the ends of the chain, we calculate, for the half-filled system, their *mutual quantum entanglement* defined as follows. We calculate the bipartite entanglement of chain A with respect to chain B [82], $S(\tilde{N}_{pf})$ for $\tilde{N}_{pf} = 2L$ (half-filled) as well as $\tilde{N}_{pf} = 2L \pm 2$. In order to distill the contribution from the boundary modes, we then subtract any residual bulk contribution by defining

$$\tilde{S} = S(\tilde{N}_{pf} = 2L) - \tfrac{1}{2}(S(\tilde{N}_{pf} = 2L + 2) + S(\tilde{N}_{pf} = 2L - 2)). \quad (17)$$

The resulting behavior is shown in Fig. 3(b). While, as is expected, the modes are unentangled (between chains A and B) at $\phi = 0$; each of these states however display a mutual entanglement of $\sim \ln(2)$ at $\phi = \pi$. This is the *central* result of this work—where ϕ, the parameter which tunes the algebra of pseudofermions, can engineer an effective interaction between the subspace of many-body boundary modes leading to nontrivial entanglement between the two physically separated SSH chains. The effective dynamics of these boundary modes, in the low-energy subspace, leads to an emergent few body quantum mechanics which we now focus on.

IV. EFFECTIVE THEORY OF THE BOUNDARY MODES

Having provided the evidence for the existence of the boundary modes for general ϕ in the half-filled system for $t_1 < t_2$, we now develop an effective theory of these many body boundary modes which are energetically separated from the extended bulk states. This effective theory as we show below is correctly captured by a two-particle problem where each of the chain is populated by just one particle residing in the boundary modes. In Fig. 3, we plot the energies of the two-particle states which are close to zero (corresponding to boundary modes) and their mutual entanglement entropy along with the results of the half-filled system. The close agreement for all $\phi \neq \pi/2$ indicates the one-to-one correspondence between the boundary modes of the two-particle system and the half-filled one as detailed below. In Sec. V, we shall discuss the phase transition at $\phi = \pi/2$ in the half-filled system which is of course a many-body bulk effect. However, both the energies and entanglement entropies for the two-particle system show extreme sensitivity to this transition as generically expected from the bulk-edge correspondence. Following our discussion near Fig. 2, at $\phi = 0$ and in the topological regime one expects four two-particle boundary states which are a direct product of single-particle boundary modes of each chain. In the next section, we discuss the effect of nonzero ϕ on these two-particle states.

A. Boundary modes and entanglement

We numerically diagonalize the Hamiltonian in Eq. (6) for the above two particle set up to obtain their energy spectrum which is plotted as a function of ϕ for both periodic and open boundary conditions in Figs. 4(a) and 4(b), respectively. Unlike the periodic system, the system with open boundary conditions shows four quasidegenerate zero energy states, labeled $(e_1 - e_4)$, whose energies are weakly sensitive to ϕ as shown in Fig. 4(c). Our choice of $\gamma = 2$ [defined above Eq. (5)] changes the relative bandwidths of the two chains in such a way that the two-particle spectrum is gapped at $E = 0$ for the periodic system, and existence of two-particle boundary modes, if any, is clearly visible.

In Fig. 4(d), we plot the local density of states (LDOS) for these four states showing that they indeed remain localized at the boundary. As remarked above, the boundary modes of the two-particle system very closely reproduces the excitation energies of the boundary of the half-filled system as was shown in Fig. 3(a). We explore this one-to-one correspondence for the boundary modes to explore their properties in greater detail. It is worthwhile to note that these two-particle boundary modes are not the ground states of the two-particle problem and are separated in energy from all two-particle bulk states by tuning γ. This is in contrast to the many-body boundary modes where such boundary modes become the quasidegenerate ground-state manifold for an half-filled system. Also given the presence of just one particle per chain the renormalization of the energies of the bulk two-particle states due to ϕ [see Fig. 4(a)] is not as drastic as the half-filled many-body states, which we discuss in Sec. V.

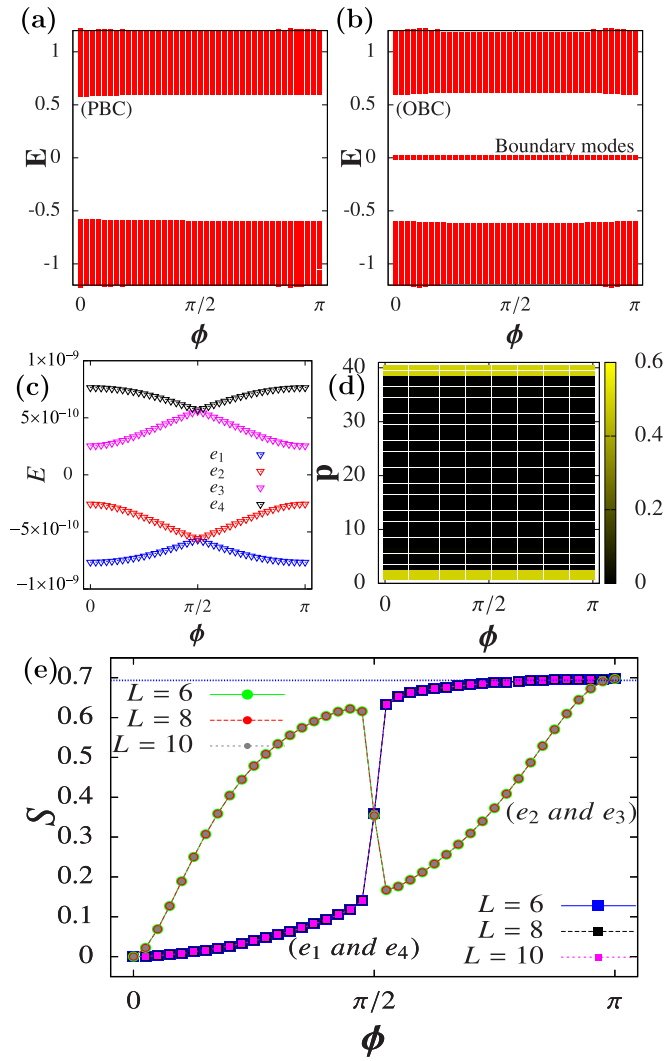

FIG. 4. Two-particle problem and boundary modes. Energies for a two-particle system under (a) periodic boundary conditions (PBC) and (b) open boundary conditions (OBC) as a function of ϕ. (c) The near-zero energy states in (b) are zoomed—showing four states (labeled $e_1 - e_4$), which disperse as a function of ϕ. (d) The combined LDOS of the four states plotted as a function of position, p show that the states close to $E = 0$ are localized at the boundaries. (e) The mutual entanglement entropy (S) between the two chains as a function of ϕ for each of the four states. They reach a value of $\ln(2)$ at $\phi = \pi$ (shown by dashed line). [ED, $t_1 = 0.1$, $t_2 = 0.9$, $\gamma = 2$ for (a)–(d) $N = 4L = 40$].

In Fig. 3(b), we plot the energies of the two-particle states which are close to zero (corresponding to boundary modes) and their mutual entanglement entropy along with the results of the half-filled system. The close agreement for all $\phi \neq \pi/2$ indicates the one-to-one correspondence between the boundary modes of the two-particle system and the half-filled one as detailed below. In Sec. V, we shall discuss the phase transition at $\phi = \pi/2$ in the half-filled system which is of course a many-body bulk effect. However, both the energies and entanglement entropies for the two-particle system show extreme sensitivity to this transition as generically expected from the bulk-edge correspondence. Following our discussion near Fig. 2, at $\phi = 0$ and in the topological regime one expects four two-particle boundary states which are a direct product of single-particle boundary modes of each chain. In the next section, we discuss the effect of nonzero ϕ on these two-particle states.

The mutual entanglement between the boundary modes of chain A and B for the two-particle system can be calculated in

a straightforward manner as follows. We perform a singular value decomposition (SVD) of the two-particle state $|\Psi\rangle$ to obtain

$$|\Psi\rangle = \sum_{i,j=0}^{2L-1} a_{ij}|2i+2\rangle|2j+1\rangle, \tag{18}$$

where $|p\rangle = c_p^\dagger|0\rangle$ is the single-particle *fermionic* state at position p with the even and odd positions belonging to chain A and B, respectively. The matrix $\mathbf{a}$ can be SVD diagonalized $\Lambda = U^{-1}\mathbf{a}V$ to obtain the diagonal eigenvalues Λ_i [83]. The $|\Psi\rangle$ then can be expressed as

$$|\Psi\rangle = \sum_j \Lambda_j|\Psi_{jA}\rangle|\Psi_{jB}\rangle, \tag{19}$$

where $|\Psi_{jA}\rangle = \sum_i U_{ij}|2i+2\rangle$ and $|\Psi_{jB}\rangle = \sum_i (V^{-1})_{ji}|2i+1\rangle$ form orthonormal vectors in single-particle Hilbert space of both the chains separately. This decomposes the wave function in a way that the two sectors correspond to two distinct chains. Λ_i characterizes the entanglement properties of this two-particle state. In particular, a direct product state has $\Lambda_i = \delta_{i,0}$. More generally the entanglement entropy between two chains is given by [83]

$$S = -\sum_j [|\Lambda_j|^2 \ln |\Lambda_j|^2]. \tag{20}$$

In Fig. 4(e), we plot S for the four boundary modes of the two-particle problem ($e_1, \ldots, e_4 < \Delta_{bw}$) (where Δ_{bw} is the bandwidth of these modes as discussed below). Interestingly, while for all the states, the chains remain unentangled at $\phi = 0$, the entanglement entropy saturate to a value of $\sim \ln 2$ at $\phi = \pi$ undergoing a jump at $\phi = \pi/2$. A systematic increase in L doesn't change this functional dependence of S on ϕ, thereby reflecting that this result is indeed stable even at the thermodynamic limit [see Fig. 4(e)]. Once again, the results of the two-particle mutual entanglement properties of the boundary modes are in one-to-one correspondence with that of the half-filled case as shown in Fig. 3(b).

It is important to contrast the above mutual (interchain) entanglement, with the intra-chain entanglement as a function of ϕ. To this end, we partition the system into three regions I–III (see inset in Fig. 5) with the bipartite entanglement between the particular part and the rest of the system being given by $S_{\rm I}$, $S_{\rm II}$, and $S_{\rm III}$, respectively. While $S_{\rm III}$ represents the mutual entanglement previously calculated [see Fig. 4(e)], $S_{\rm I}$ represents the entanglement entropy of the left part of chain B with the rest of the system. Figure 5 shows that $S_{\rm I}$ remains close to ln(2) as a function of ϕ indicating that the left boundary mode in B continues to remain entangled throughout—as is expected in a topological phase. We further calculate

$$S_{\rm ex} = S_I - S_{\rm III}, \tag{21}$$

which represents the exclusive entanglement entropy between regions I and II. At $\phi = 0$, given the ground state is in a direct product state of two electrons residing in bonding orbitals in each of the chains, the entanglement entropy between left half of chain A (B) and right half of chain A (B) is expected to be ln(2) which is confirmed in Fig. 5 for $\phi < \pi/2$. However, as seen in the figure, $S_{\rm ex}$ jumps from $\sim \ln(2)$ to $\sim$zero at $\phi = \frac{\pi}{2}$

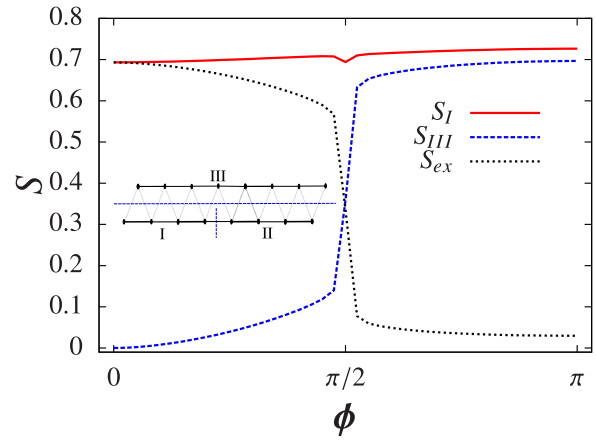

FIG. 5. Intrachain entanglement. The behavior of entanglement entropy $S_{\rm I}$, $S_{\rm III}$, and $S_{\rm ex}$ [see Eq. (21)] (the regions I–III are shown in the inset) as a function of ϕ for the two-particle system in the topological regime for the two-particle state e_1 [see Fig. 4(c)]. (ED, $t_1 = 0.1$, $t_2 = 0.9$, $\gamma = 2$, and $N = 4L = 16$).

(see Fig. 5). The almost perfect anticorrelation between $S_{\rm ex}$ and $S_{\rm III}$ shows that as the chains get mutually entangled, the exclusive entanglement between left and right parts of chain B (A) goes to zero in accordance with the monogamy of entanglement for the boundary modes akin to spin $S = 1/2$ degree of freedom or spinless fermions.

B. Minimal model for the boundary modes

In order to develop possible protocols to manipulate the boundary modes for finite chains, it is desirable to develop an effective description only involving them that is operational at energy scales much below the bulk gap. This takes the form of an effective few particle quantum mechanics with subtle features resulting from the underlying nontrivial nature of the bulk stemming from the underlying topological phase. In our case, this leads to a four-site quantum mechanics whose features can be controlled by tuning ϕ.

For a single finite SSH chain [see Eq. (9)] in its topological phase, there are two nearly degenerate eigenstates close to zero energy. These are the bonding (+) and the antibonding (−) orbitals formed out of the linear combination of the boundary modes

$$c_+^\dagger = \frac{1}{\sqrt{2}}(c_L^\dagger + c_R^\dagger), \quad c_-^\dagger = \frac{1}{\sqrt{2}}(c_L^\dagger - c_R^\dagger), \tag{22}$$

where $c_L^\dagger(c_R^\dagger)$ creates an exponentially localized wave function on left (right) edge of the chain. c_+ and c_- are energetically split by energy [84]

$$\alpha \approx \frac{t_1 t_2^2}{t_1^2 + t_2^2} e^{-(L-1)/\zeta}, \tag{23}$$

where $\zeta = 1/\ln(t_2/t_1)$. Therefore, an effective Hamiltonian for *just* the boundary modes of a single SSH chain is $H_{\rm eff} = -\alpha(c_L^\dagger c_R + \text{H.c.})$.

For two chains A and B, we similarly have four single-particle degrees of freedom $(c_{L,(A/B)}^\dagger, c_{R,(A/B)}^\dagger)$ corresponding to left and right boundary modes on each chains A and B.

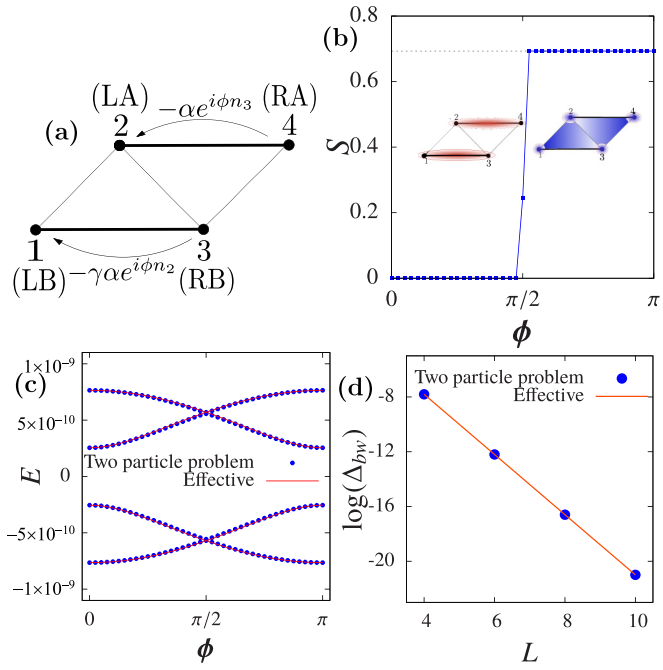

FIG. 6. Minimal four-site model. (a) Schematic of the four-site model of the boundary modes. (b) Entanglement jump of ln(2) as a function of ϕ for the ground state of the four-site system [Eq. (25) with $\gamma = \alpha = 1$] that changes from an unentangled state [Eq. (27), two red-colored bonding orbitals] to an mutually entangled state (Eq. (28), blue-shaded plaquette]. (c) For actual choice [see Eq. (23)] of α and γ in Eq. (25), the spectra of this four-site problem compared to the two-particle boundary modes ($t_1 = 0.1,\ t_2 = 1 - t_1,\ \gamma = 2$, and $N = 4L = 40$). (d) Behavior of the bandwidth of boundary modes (Δ_{bw}) from the two-particle problem and its comparison to that obtained from the effective Hamiltonian in Eq. (25), as a function of system size L.

Identifying $c^\dagger_{LB}$, $c^\dagger_{LA}$, $c^\dagger_{RB}$, and $c^\dagger_{RA}$ with four "effective sites" $\equiv (1, 2, 3, 4)$ of a four site cluster [see Fig. 6(a)], we form a two particle basis given by

$$|1,2\rangle \equiv |LB, LA\rangle, \quad |1,4\rangle \equiv |LB, RA\rangle,$$
$$|3,2\rangle \equiv |RB, LA\rangle, \quad |3,4\rangle \equiv |RB, RA\rangle, \tag{24}$$

which reflects that both the chains have one particle each.

In order to uncover the effective dynamics among these boundary modes, as tuned by ϕ dependent correlated hopping term, one can consider the case where a particle localized at right boundary of chain A (RA - "site 4") is brought to the left boundary (LA -"site 2") via a hopping process $\propto t_1(t_1t_2)^{L-1}$. However, in the process the ϕ dependent term would contribute an overall phase which depends on the number density on the chain B up until it encounters the left boundary of chain B. This should lead to an effective term of the kind $\sim c^\dagger_2 c_4 e^{i\phi n_3}$ since n_3 measures the density on the right boundary of chain B. Similarly considering the equivalent process on the other chain, the effective Hamiltonian at any ϕ is given by

$$H_{\text{eff}} = -\alpha e^{\mathbb{i}\phi n_3} c^\dagger_2 c_4 - \gamma\alpha e^{\mathbb{i}\phi n_2} c^\dagger_1 c_3 + \text{H.c.}, \tag{25}$$

where $\gamma\alpha$ is the magnitude of the corresponding energy splitting between the boundary modes of the (finite) chain B ($t'_1 = \gamma t_1,\ t'_2 = \gamma t_2$). The effective Hamiltonian, for $\phi = 0$, reduces to

$$H_{\text{eff}}(\phi = 0) = -\alpha(c^\dagger_{LA} c_{RA} + \text{H.c.}) - \gamma\alpha(c^\dagger_{LB} c_{RB} + \text{H.c.}), \tag{26}$$

which is trivially two copies of the edge Hamiltonian for two decoupled SSH chains, A and B. It is interesting to note that the four-site effective Hamiltonian of the boundary modes [see Eq. (25)] is also the Hamiltonian for a single unit cell comprising of four sites in our parent Hamiltonian when $\alpha = t_1, t_2 = 0$ [see Eq. (6)].

The eigenspectrum of H_{eff} and the mutual entanglement of the states (given a choice of t_1, t_2, γ, L) matches with the results for the full system almost exactly. The comparison of the eigenspectra for this effective four-site model and that of the boundary modes from the exact two-particle system is shown in Fig. 6(c). Furthermore the fact that the dispersion of the boundary modes for this two-particle system and its entanglement properties almost exactly matches the corresponding features of many-boundary modes (see Fig. 3) shows that Eq. (25) is the effective Hamiltonian for the many-body boundary modes in this system as tuned by ϕ. The discussion above also provides for the effective bandwidth of the two particle boundary states (Δ_{bw}) given by $2|\alpha + \gamma\alpha|$, which, as expected, falls off exponentially with L [see Fig. 6(d)]. Given the exponential fall in Δ_{bw} with increasing L, it is pertinent; especially in an experimental setting, to maintain L and ζ length scales which can allow for tunability between the boundary modes even while resolving their individual energies. Apart from energetic scale α and the anisotropy factor γ which denote the finite hybridization between the boundary modes of the finite chain, it is the presence of ϕ—reflecting a correlated hopping process—that plays the central role in the effective boundary physics and entanglement characteristics.

To understand this, we momentarily set $\alpha = \gamma = 1$ in Eq. (25). The resultant ground state is given by

$$|\Psi_1\rangle = \left(\frac{e^{\mathbb{i}\frac{\phi}{2}} c^\dagger_1 + c^\dagger_3}{\sqrt{2}}\right)\left(\frac{e^{\mathbb{i}\frac{\phi}{2}} c^\dagger_2 + c^\dagger_4}{\sqrt{2}}\right)|\Omega_2\rangle \tag{27}$$

$\forall\ \phi < \pi/2$ and

$$|\Psi_2\rangle = \tfrac{1}{2}(-e^{\mathbb{i}\phi} c^\dagger_1 c^\dagger_2 - \mathbb{i} e^{\mathbb{i}\phi/2} c^\dagger_1 c^\dagger_4 + \mathbb{i} e^{\mathbb{i}\phi/2} c^\dagger_3 c^\dagger_2 + c^\dagger_3 c^\dagger_4)|\Omega_2\rangle \tag{28}$$

$\forall\ \phi > \pi/2$, where $|\Omega_2\rangle$ describes the vacuum state of the effective quantum mechanics of the boundary modes. At $\phi = \pi/2$ the above two states are energetically degenerate and the corresponding energy-levels cross at $\phi = \pi/2$. In this case, for the ground state, up until $\phi = \pi/2$ the mutual entanglement between the two chains is identically zero and then jumps to ln(2) at $\phi = \frac{\pi}{2}$ [showed by dashed line in Fig. 6(b)]. This is expectedly so, given the form of $|\Psi_1\rangle$ [see Eq. (27)] is a direct product state between the two chains which can be shown schematically by two disjoint bonding-like orbitals on the two chains. This is to be contrasted with $|\Psi_2\rangle$ [see Eq. (28)], which is an entangled state [shown schematically in Fig. 6(b)] where even when fermions are delocalized equally among the four sites, the state cannot be represented as a direct product (as shown by a blue shaded plaquette).

Therefore we show that the effective low-energy physics of the many-body boundary modes (which in turn was captured

TABLE I. Eigenvalues of the symmetry operators U_e and U_o [Eqs. (12) and (13)] for the two eigenstates $|\Psi_1\rangle$ and $|\Psi_2\rangle$ [see Eqs. (27) and (28)]. $|\Psi_1\rangle$ ($|\Psi_2\rangle$) is the ground state for $\phi < \frac{\pi}{2}$ ($\phi > \frac{\pi}{2}$) for the effective Hamiltonian [see Eq. (25)] when $\alpha = \gamma = 1$.

	$\|\Psi_1\rangle$	$\|\Psi_2\rangle$
U_o	$e^{-i5\phi/2}$	$ie^{-i5\phi/2}$
U_e	$e^{-i2\phi}$	$-ie^{-i2\phi}$

by the physics of two-particle boundary modes; see Fig. 3); is actually that of a correlated hopping in a four-site cluster, albeit nonlocal. This allows for the entanglement tuning of the nonlocal modes that is facilitated by the nontrivial bulk (see Fig. 3).

At this point, we note that $|\Psi_1\rangle$ and $|\Psi_2\rangle$ are in fact eigenstates of the two symmetry operators U_o and U_e defined in Eqs. (12) and (13) with the eigenvalues shown in the Table I. The level crossing at $\phi = \frac{\pi}{2}$, which leads to an entanglement jump, is therefore a reflection of the change in the symmetry representation of the ground state as ϕ is tuned above $\phi = \frac{\pi}{2}$. We shall discuss the implication of these ideas further in Sec. V where we discuss the underlying phase transition in the many-body system.

We now briefly comment on a possible experimental protocol to measure the above mutual entanglement [Fig. 4(e)] relevant to recent experiments [46,47] and especially applicable in this two particle setting. Following Ref. [85], the setup comprises of engineering a quantum switch with two states denoted by $|\uparrow\rangle, |\downarrow\rangle$ coupled to the Hamiltonian [see Eq. (6)]. Now consider two values of the statistical parameter ϕ and ϕ' such that the complete system (SSH chains and the switch) is prepared in the ground states $|\uparrow\rangle \otimes |\Psi(\phi)\rangle$ and $|\downarrow\rangle \otimes |\Psi(\phi')\rangle$ where $|\Psi(\phi)\rangle$ and $|\Psi(\phi')\rangle$ are the ground states for $H(\phi)$ and $H(\phi')$, respectively. A system in $|\Psi(\phi)\rangle$ can be made to oscillate via Rabi oscillations to a state $|\Psi(\phi')\rangle$ using a tunneling term of the form $H' = \Gamma(|\uparrow\rangle\langle\downarrow| + |\downarrow\rangle\langle\uparrow|)$ on the quantum switch. This leads to a characteristic Rabi frequency Ω where $\Omega = \frac{\Gamma'}{\hbar}$ and $\Gamma' = \Gamma\langle\Psi(\phi)|\Psi(\phi')\rangle$ [85], which can then be experimentally measured. Note that this quantity is dependent on the overlap $\chi(\phi, \phi') = \langle\Psi(\phi)|\Psi(\phi')\rangle$.

In order to track a mutually entangled state, it is particularly useful to discuss two choices of ϕ and ϕ': (a) $\phi = 0$ and $\phi' = \pi$ where the $\chi(0, \pi) = \frac{1}{2}$ [calculated using the forms of wave functions shown in Eqs. (27) and (28)] and (b) $\phi = \epsilon(\sim 0)$ and $\phi' = -\epsilon$ where $\chi \sim 1$. Note that the ground state for each of these values of ϕ and ϕ' have the same energy. However, the measurement of Rabi oscillations in (a) is half of that measured in (b). Unlike case (b), in case (a), $|\Psi(\phi')\rangle$ is an mutually entangled state. This characteristic halving of Ω would therefore signal generation of nontrivial *mutual entanglement* between chains A and B. While this result is expected for the four site cluster, and for the boundary modes for the two-particle problem—in a many-body problem $\chi(\phi, \phi')$ falls exponentially with increasing system size (as we have checked numerically using many-body wave functions) rendering such a protocol potentially challenging to implement in an experimental setting.

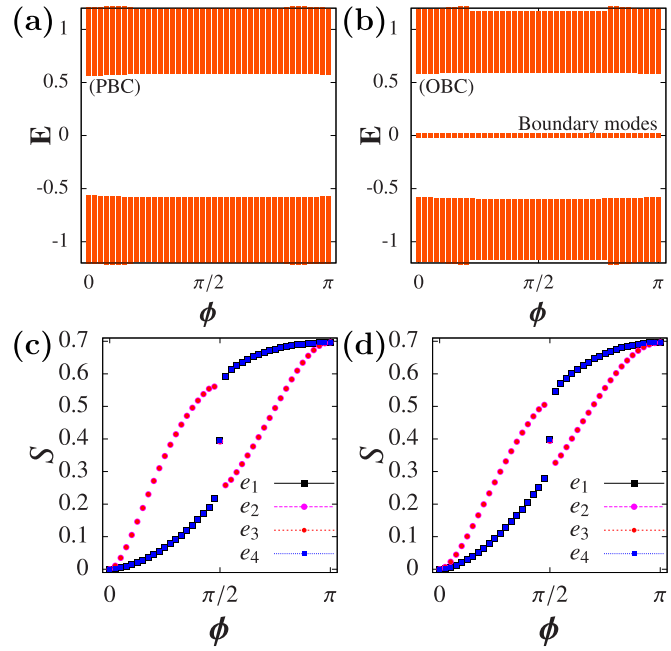

FIG. 7. Stability to hopping disorder. [(a) and (b)] The energy spectra for a two-particle problem as a function of ϕ with hopping disorder strength $W = t_1/5$ under (a) periodic boundary conditions (PBC) and (b) under open boundary conditions (OBC). [(c) and (d)] The jump in mutual entanglement S as a function of ϕ for the four two-particle boundary modes $(e_1, \ldots, e_4)$ for disorder strength (c) $W = t_1/10$ and (d) $W = t_1/5$. (ED, $t_1 = 0.1$, $t_2 = 0.9$, $\gamma = 2$, and $N = 4L = 40$).

C. Stability to disorder and other perturbations

While our discussion until this point describes the existence of boundary modes and their tunability with respect to ϕ, their topological origin should impart them stability against symmetry preserving disorder and other perturbations. Here we examine these effects in turns starting with the disorder.

For hopping disorder, the hopping amplitudes, i.e., various t in Eq. (6) are modified to $\tilde{t} = t + \delta t$ where a small random number (δt) is uniformly drawn from a box distribution between $[-W, W]$ independently for each bond. We find that such a disorder does not destroy the boundary modes and their entanglement properties (see Fig. 7) for the two particle problem. We have also checked that this property holds even for the many-body boundary modes (not shown). In contrast to site disorder [86], hopping disorder retains the generalized charge-conjugating symmetries U_e and U_o separately. However, such protection of boundary modes is guaranteed only until the point when the disorder scale is weak compared to the bulk gap scale in the system whence it drives a bulk phase transition to a trivially localized phase. In that limit, both topological features and corresponding entanglement entropy changes significantly (also seen in other systems such as [87,88]) (see Appendix B for a detailed discussion).

We now turn to the role of *translationally invariant* symmetry preserving and symmetry breaking perturbations to Eq. (6). Specifically, we study the effect of Hubbard

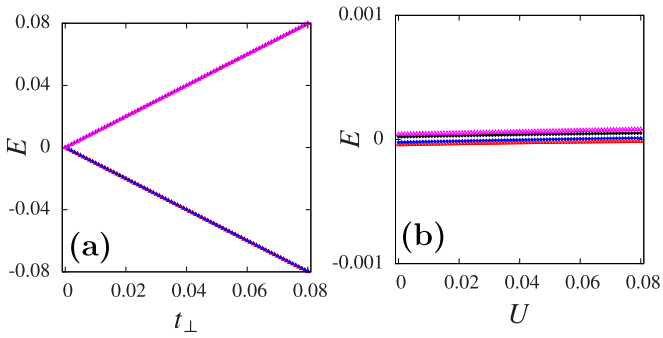

FIG. 8. Symmetry breaking/preserving perturbations. (a) Energies of the single-particle boundary modes as a function of interchain hopping strength $t_\perp$ at $\phi = 0$ [see Eq. (30)]. (b) Energies of boundary modes in presence of two particles, as a function of Hubbard interaction strength U [see Eq. (29)] at $\phi = \pi/4$. Here, an overall constant proportional to U is subtracted. (ED, $t_1 = 0.1$, $t_2 = 1 - t_1$, $\gamma = 2$, and $N = 4L = 20$).

interaction given by

$$H_U = \frac{U}{2}\sum_{i=0}^{L-1}[(\tilde{n}_{4i+1} + \tilde{n}_{4i+2} + \tilde{n}_{4i+3} + \tilde{n}_{4i+4})^2 - 1] + U\sum_{i=0}^{L-1}[(\tilde{n}_{4i+4} + \tilde{n}_{4i+3})(\tilde{n}_{4(i+1)+1} + \tilde{n}_{4(i+1)+2})], \quad (29)$$

where $\tilde{n}_p = n_p - \frac{1}{2}$ and the interaction term coupling the $i = (L-1)$ and the $i = 0$ unit cell is kept such that the perturbing term does not break the symmetry of the parent periodic system. While this term is invariant under a product of U_o and U_e, it is not invariant under them separately. This term further maintains the $U_A(1) \times U_B(1)$ number conservation symmetry of the system. Upto an overall chemical potential renormalization we find that the boundary modes do not split and remain quasi degenerate (exponentially close in system size $\sim e^{-L/\zeta}$). This can be contrasted with the case when the system is perturbed by an interchain hopping term of the kind

$$H_{t_\perp} = -\sum_{i=0}^{L-1} t_\perp(c^\dagger_{4i+1}c_{4i+2} + c^\dagger_{4i+2}c_{4i+3} + c^\dagger_{4i+3}c_{4i+4} + c^\dagger_{4i+4}c_{4(i+1)+1} + \text{H.c.}). \quad (30)$$

Here $t_\perp$ breaks U_o, U_e, U_oU_e and $U_A(1) \times U_B(1)$ symmetries. We find that such a perturbation immediately splits the boundary modes [see Fig. 8(a)].

The two distinct behaviors for the two kinds of perturbations can be understood from the effective Hamiltonian for the boundary modes as discussed in Eqs. (26) and (25). $H_{t_\perp}$ effectively generates a hopping term of the kind

$$H_{t_\perp} = -t_\perp(c^\dagger_{LB}c_{LA} + c^\dagger_{RB}c_{RA} + \text{H.c.}) \quad (31)$$

immediately hybridizing the boundary modes, while H_U generates a term of the kind

$$H_U = U(\tilde{n}_{LB}\tilde{n}_{LA} + \tilde{n}_{LB}\tilde{n}_{RA} + \tilde{n}_{RB}\tilde{n}_{LA} + \tilde{n}_{RB}\tilde{n}_{RA}), \quad (32)$$

which acts as an identity term in Eq. (25). Given the two distinctive behaviors of these perturbing terms, this analysis shows that the symmetry protecting this topological phase is rather a product of two antiunitary operators U_oU_e, in combination with the number conservation $U_A(1) \times U_B(1)$.

This completes our discussion of the effective quantum mechanics of the boundary modes. Our discussion of the two-particle problem shows existence of quasidegenerate eigen-modes in an open system when $t_1 < t_2$, which reside on the boundaries and are robust to disorder and symmetry preserving perturbations; taken together, these results provide a comprehensive understanding that these modes are indeed of topological origins at any value of ϕ. In this section, we further discussed their effective dynamics in presence of ϕ, their entanglement properties and potential measurement protocols.

Having discussed this interplay of statistics, entanglement and symmetries—on the boundary modes of this topological phase, we now turn to the many-body problem and discuss the bulk physics of the half-filled system and understand its properties as a function of ϕ.

V. MANY-BODY SYSTEM

The trivial and topological phase of a single SSH chain [see for e.g., Eq. (9)] is distinguished by the value of polarization (defined modulo 2)

$$P = \frac{1}{\pi}\text{Im}\left[\ln\left(\left\langle\exp\left(\mathbb{i}\frac{2\pi}{L}\sum_{i=0,\ldots,L-1}^{j=1,2} x_i n_{2i+j}\right)\right\rangle\right)\right], \quad (33)$$

where i runs over the unit cell index and j over the sites within a unit cell and x_i describes the position of the ith unit cell [89–92]. Also $\langle\cdots\rangle$ denotes expectation is taken over the many-body ground state of the system. The resulting value of polarization can be related to the geometric phase of the single-particle bands in an noninteracting system [90]. Given, presence of a nontrivial ϕ engineers interactions which does not allow the description of the many-body state in terms of single Slater determinant; here, while one can not evaluate a single-particle geometric phase (and corresponding winding number)—but a many-body polarization can still be calculated for the half-filled system as follows.

For our two-chain system, we calculate the polarization for each chain separately (P_A and P_B) given by

$$P_A = \frac{1}{\pi}\text{Im}\left[\ln\left(\left\langle\exp\left(\mathbb{i}\frac{2\pi}{L}\sum_{j=2,4}^{i=0\ldots L-1} x_i n_{4i+j}\right)\right\rangle\right)\right],$$
$$P_B = \frac{1}{\pi}\text{Im}\left[\ln\left(\left\langle\exp\left(\mathbb{i}\frac{2\pi}{L}\sum_{j=1,3}^{i=0\ldots L-1} x_i n_{4i+j}\right)\right\rangle\right)\right]. \quad (34)$$

We find that the values when evaluated over the ground state (defined modulo 2) continues to be nontrivially 1 as a function of ϕ when $t_1 < t_2$ [see Fig. 9 (a)]. It is not well defined at $\phi = \frac{\pi}{2}$ owing to a level crossing of the ground states which we shall shortly discuss. Our results therefore show that the many body topological phase which exists at $\phi = 0$ is indeed stable all the way up to $\phi = \pi$ remaining independent of ϕ. Therefore we have not been able to find a topological invariant that distinguishes $\phi < \frac{\pi}{2}$ and $\phi > \frac{\pi}{2}$ regions.

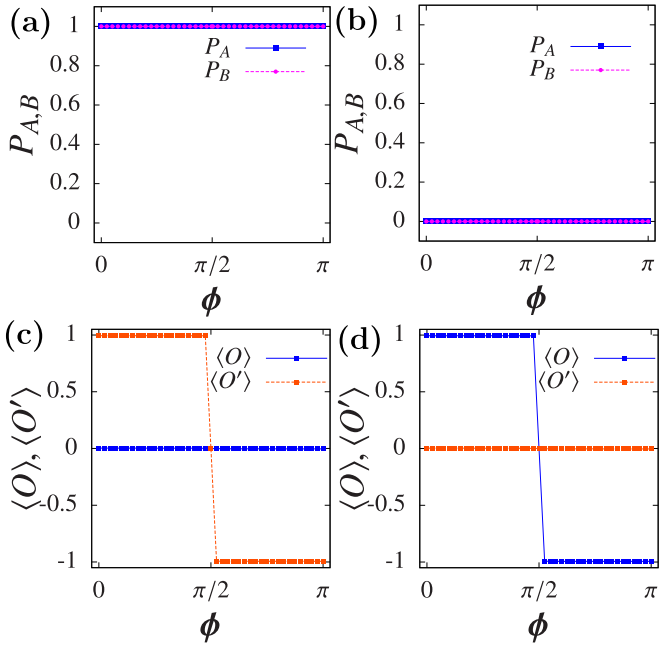

FIG. 9. Polarization. The behavior of P_A and P_B [see Eq. (34)] with respect to ϕ for (a) $t_1 = 0.1$ (topological phase) (b) $t_1 = 0.9$ (trivial phase) (see text). The behavior of $\langle O \rangle$, $\langle O' \rangle$ [see Eq. (35)] as a function of ϕ in (c) $t_1 = 0.1$ and (d) 0.9. (ED, $t_2 = 1 - t_1$, $\gamma = 1$, and $N = 4L = 16$).

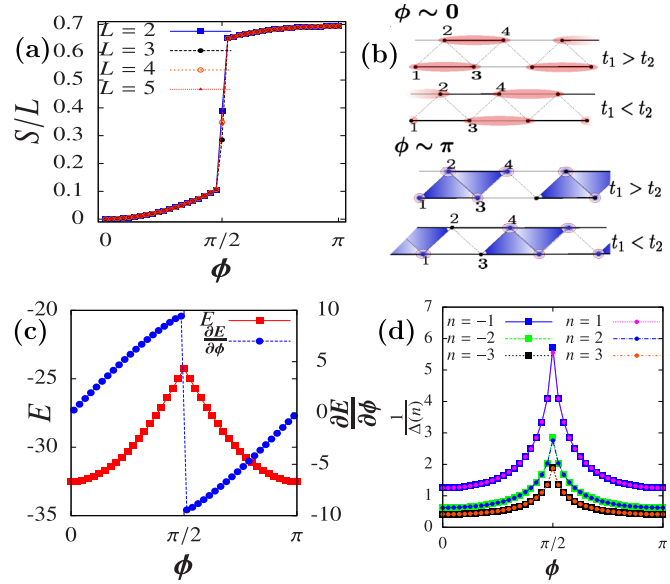

FIG. 10. Half-filled periodic system. (a) The behavior of mutual entanglement entropy S as a function of ϕ shows a jump of $L \ln(2)$ at $\phi = \frac{\pi}{2}$ for different system sizes. (b) Schematic showing that the ground state for $t_1 \ll t_2$ and $t_1 \gg t_2$ can be interpreted as weakly coupled four-site clusters of unentangled states at $\phi \sim 0$ and entangled states at $\phi \sim \pi$. (c) Ground-state energy E and its derivative with respect to ϕ ($\frac{\partial E}{\partial \phi}$) as a function of ϕ. (d) Behavior of $1/\Delta(n)$ (see Eq. (36)) as a function of ϕ. For (a) ED studies and for (c) and (d) $N = 4L = 48$, DMRG calculations further details in Appendix A). ($t_1 = 0.1$, $t_2 = 0.9$, and $\gamma = 2$, PBC).

Even as polarization remains nontrivial, is there another operator which differentiates the bulk phase $\phi < \frac{\pi}{2}$ and $\phi > \frac{\pi}{2}$? To construct such operators we draw insights from our study of the four-site problem which was introduced as an effective problem for the boundary modes in Eq. (25). While there these four "sites" represented the effective boundary modes (see Fig. 6); this effective Hamiltonian is also identical to the terms which appear in the Hamiltonian of a single unit cell (comprising of four sites) in our correlated fermionic Hamiltonian [see Eq. (6)]. Specially at $t_2 = 0$ limit, our complete system can be understood as a direct product of four-site clusters, each of which satisfies the Hamiltonian (25) with $\alpha = t_1$. Motivated by this connection we construct the following Hermitian operators, both of which commute with U_o and U_e:

$$O = \frac{1}{L}\sum_i \left[e^{i\frac{\phi}{2}} c^\dagger_{4i+1} c_{4i+3} + \text{H.c.}\right]\left[e^{i\frac{\phi}{2}} c^\dagger_{4i+2} c_{4i+4} + \text{H.c.}\right],$$

$$O' = \frac{1}{L}\sum_i \left[e^{i\frac{\phi}{2}} c^\dagger_{4i+3} c_{4i+5} + \text{H.c.}\right]\left[e^{i\frac{\phi}{2}} c^\dagger_{4i+4} c_{4i+6} + \text{H.c.}\right]. \tag{35}$$

$\langle O \rangle$ for a single four site cluster has an value $+1(-1)$ for ground-state wave function $|\Psi_1\rangle(|\Psi_2\rangle)$ [see Eqs. (27) and (28)] and O' is displaced by half a unit cell from O. While at $\phi = 0$, O is a product of two hopping operators on the two bonds of chains A-B, at $\phi = \pi$, they appear as product of two current operators between the two chains. For a many-body system, these effectively measures the location and the phase relationship of fermions on the bonds of the two chains, respectively. Indeed for $\phi = 0$, $\langle O \rangle = 0$ ($\langle O' \rangle = 1$) in the topological phase ($t_1 < t_2$) and other way around in the nontopological phase ($t_1 > t_2$). Interestingly *even in the topological (trivial) phase, as ϕ is tuned, the sign of $\langle O' \rangle$ ($\langle O \rangle$) changes at $\phi = \frac{\pi}{2}$* [see Figs. 9(c) and 9(d)]. This signals the nontrivial phase relationship of the bonding orbitals which is tuned by ϕ and suddenly changes its character at $\phi = \frac{\pi}{2}$.

A. Entanglement and gap

In a system with open boundary conditions we had found that ϕ engineered a jump in the mutual entanglement between the boundary modes belonging to the two chains. In a periodic system, the ground state is unique (except at $\phi = \frac{\pi}{2}$) and we now investigate the behavior of mutual entanglement between the two chains in this ground state as a function of ϕ. We find that such mutual entanglement jump continues at $\phi = \frac{\pi}{2}$, but with a value of $L \ln(2)$, which is *extensive* in system size [see Fig. 10(a)] given L is the number of four-site unit cells. This suggests that this entanglement is engineered through bulk states—where each unit cell contributes a value of $\ln(2)$. This reflects what we had found as the properties of a single four-site cluster as discussed near Eq. (25). The transition for the many-body state thus provides a natural understanding of the state, where deep in both the topological regime ($t_1 \ll t_2$) and trivial regime ($t_1 \gg t_2$), the state can be interpreted as weakly coupled four-site clusters each of which contributing a $\ln(2)$ entropy [see Figs. 6(a) and 6(b)] to the many-body state once $\phi > \frac{\pi}{2}$ [see Fig. 10(b)]. This also provides the understanding for the effective four-site problem. This entanglement jump,

as we have discussed above, is not specific to the topological phase; for instance even between the two trivial phases, ϕ can engineer an entanglement jump. Furthermore, while characterization of entanglement entropy depends on the microscopic degree of freedom used (for instance, fermions or hard-core bosons), once defined with a chosen basis, its value and variation with ϕ is physical.

The sudden jump in entanglement at $\phi = \frac{\pi}{2}$ hints at an underlying thermodynamic phase transition. This is further confirmed by the behavior of the ground-state energy as a function of ϕ and find that its first-order derivative shows a distinctive jump at $\phi = \frac{\pi}{2}$, reflecting that the transition is of *first-order* [see Fig. 10(c)]. Interestingly even though system undergoes this first-order transition the single-particle gap $\Delta(n)$ defined as energy required to add or remove n particles from the half-filled sector

$$\Delta(n) = E(\tilde{N}_{pf} = 2L + n) - E(\tilde{N}_{pf} = 2L), \tag{36}$$

where E is the ground-state energy for $\tilde{N}_{pf}$ particles in a system of L unit cells, remains finite as a function of ϕ across the tuning range [see Fig. 10(d)]. That these gaps remain finite even as the system size is systematically increased (see Appendix A for details) shows that even when ϕ entangles the boundary modes and the bulk remains gapped to single-particle excitations, the ground state undergoes a level crossing.

B. Trial many-body wave functions

Motivated by the structure of the wave functions in the free SSH limit as well as that of the effective boundary Hamiltonian Eq. (25), we propose the following trial wave functions for the many-body ground state for the Hamiltonian in Eq. (6) with $t_1 = \gamma = 1, t_2 = 0$.

$$|\Psi_1^{(L)}\rangle = \prod_{i=0}^{L-1} \left(\frac{e^{\mathbb{i}\frac{\phi}{2}} c_{4i+1}^\dagger + c_{4i+3}^\dagger}{\sqrt{2}} \right) \left(\frac{e^{\mathbb{i}\frac{\phi}{2}} c_{4i+2}^\dagger + c_{4i+4}^\dagger}{\sqrt{2}} \right) |\Omega\rangle \tag{37}$$

for $\phi < \pi/2$ and

$$|\Psi_2^{(L)}\rangle = \prod_{i=0}^{L-1} \Big[\frac{1}{2} \big(- e^{\mathbb{i}\phi} c_{4i+1}^\dagger c_{4i+2}^\dagger - \mathbb{i} e^{\mathbb{i}\frac{\phi}{2}} c_{4i+1}^\dagger c_{4i+4}^\dagger + \mathbb{i} e^{\mathbb{i}\frac{\phi}{2}} c_{4i+3}^\dagger c_{4i+2}^\dagger + c_{4i+3}^\dagger c_{4i+4}^\dagger \big) \Big] |\Omega\rangle \tag{38}$$

for $\phi > \pi/2$. Here $|\Omega\rangle$ is the many-body vacuum.

The overlap with the exact ground-state for the half-filled system (even when $t_1 \neq 1.0$), as obtained from ED, with $|\Psi_1^{(L)}\rangle$ ($|\Psi_2^{(L)}\rangle$) for $0 \leqslant \phi < \pi/2$ ($\pi/2 < \phi \leqslant \pi$) is notably high as shown in Fig. 11(a). The corresponding comparison of energies are shown in Fig. 11(b). This reflects that the ground-state wave function is indeed well approximated by weakly coupled four site cluster wave functions which are unentangled between chains A and B at $\phi = 0$. However, as ϕ is tuned, these unentangled chains become entangled all throughout the bulk at $\phi = \frac{\pi}{2}$ undergoing the first-order transition. It is interesting to note that at $\phi = 0$ and $t_1 = 1$, one has an extremely large degeneracy at many-body zero energy, given each four site cluster has energy eigenvalues given by

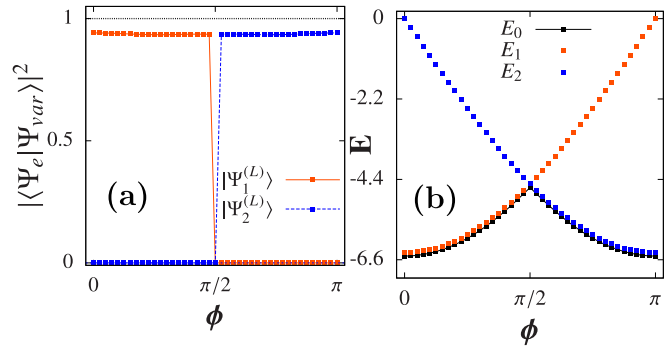

FIG. 11. Trial wave functions. (a) The behavior of the overlap ($\equiv |\langle\Psi_e|\Psi_{\text{var}}\rangle|^2$) for the two choices of trial wave functions $|\Psi_{\text{var}}\rangle = |\Psi_1^{(L)}\rangle, |\Psi_2^{(L)}\rangle$ [see Eqs. (37) and (38)] with the exact ground-state wave function $|\Psi_e\rangle$ as a function of ϕ. (b) Comparison of the corresponding energies for the trial wave functions ($E_1 = \langle\Psi_1^{(L)}|H|\Psi_1^{(L)}\rangle$, $E_2 = \langle\Psi_2^{(L)}|H|\Psi_2^{(L)}\rangle$) and the exact ground-state energy ($E = \langle\Psi_e|H|\Psi_e\rangle$) as a function of ϕ. (ED, $t_1 = 0.8 = 1 - t_2$, $\gamma = 1$, and $N = 4L = 16$).

$-2, 0, 0, 2$. The many-body spectrum can take at least $\binom{L}{\frac{L}{2}}$ (assuming L is even) number of zero energy many-body states. However ϕ chooses a particular combination of entangled states to engineer the many-body state which then forms the ground state when $\phi > \frac{\pi}{2}$. Therefore it is this change of ground-state wave function that is reflected both in the first-order transition, the jump in entanglement and corresponding jump in the value of the operators O, O' (see Fig. 9). Unlike a finite temperature first-order transition, which occurs with a latent heat corresponding to jump in the thermodynamic entropy; this quantum first-order transition occurs with a jump in the mutual entanglement entropy.

C. Breaking of $U_A(1) \times U_B(1)$ symmetry

In the last section our ED, DMRG and studies using trial wave functions convincingly point to a first-order transition, which can be engineered using ϕ. Importantly, in a system with open boundary conditions ϕ allows one to tune the entanglement properties of the many-body boundary modes (Fig. 3). The crucial symmetry protecting this physics has been $U_o U_e$ [see Eqs. (12) and (13)] and the number conservation $U_A(1) \times U_B(1)$ on each chain as was discussed in Sec. IV C. In Sec. IV C, we had looked at the effect of symmetry-breaking and symmetry-preserving perturbations on the two-particle problem and found that boundary modes would split in presence of an interchain hopping of strength $t_\perp$ (see Fig. 8). In particular for this interchain hopping, the splitting is $\propto t_\perp$ which is a much larger scale compared to the finite size splitting scale at $t_\perp = 0$ which is exponential small in system size. However, the actual mixing depends on the strength of perturbations with respect to the bulk gap and the boundary modes may survive for practical purposes for small perturbations, albeit now split. This occurs especially when the perturbing energy scales and probe fields are much smaller than the bulk gap. In this section, we investigate such features and potential signatures which would be experimentally measurable even in presence of weak interchain hopping—

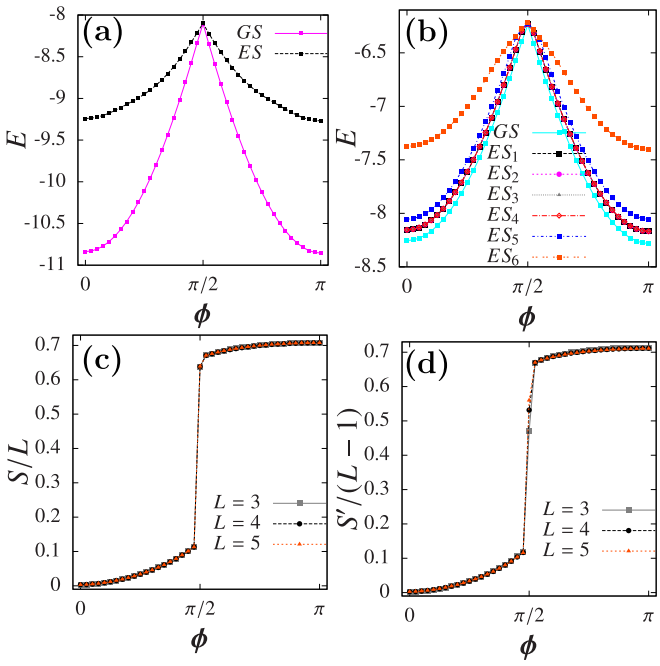

FIG. 12. Breaking $U_A(1) \times U_B(1)$. (a) Energies of the ground state and first excited state (GS and ES) as a function of ϕ for a half-filled system under periodic boundary conditions (PBC) in presence of interchain hopping $t_\perp$ [see Eq. (30)]. (b) Energies of the seven low lying energy states (GS and $ES_1 - ES_6$) for the same system but under open boundary conditions (OBC). (c) Behavior of entanglement entropy S as a function of ϕ for the ground state under PBC for various system sizes. (d) Behavior of bulk entanglement entropy $S' = S - 2\ln 2$ as a function of ϕ for various system sizes. [ED, $t_1 = 0.1, t_2 = 0.9, t_\perp = t_1/2, \gamma = 2$, for (a) and (b), $N = 4L = 16$].

particularly when, such terms may be realistically present in any experimental setting [46].

In order to study this we add a quadratic hopping term $t_\perp$ [see Eq. (30)] along dashed lines (see Fig. 1) to the parent Hamiltonian [Eq. (6)] and perform ED studies on the many-body problem. Given the number of particles on each chain are no longer conserved, simple counting in the free fermionic limit shows that one would expect *six* low-energy states in an open system (six ways of occupying boundary modes) when both the chains are in topological regime (instead of four as discussed before) and expect a unique ground state with a finite gap to excitations in a periodic system. This expectation is borne out in the ED studies [see Figs. 12(a) and 12(b)] where the many-body energy spectra for both periodic and open system is shown. In particular, we find that the low-energy manifold in the open system is not exactly degenerate, but split ($\propto t_\perp$) due to a finite $t_\perp$ [consistent with results in Sec. IV C]. However, these lowest six eigenstates still remains separated in energy to bulk excitations with an energy scale $t_1 - t_2$ that characterizes the bulk gap scale. This gap scale is characterized by the energy of the transition from ground state to sixth excited state, which remains finite [see Fig. 12(b)], except when near $\phi = \frac{\pi}{2}$ where the first-order phase transition occurs.

We now investigate if the entanglement properties of the many-body states remain stable to interchain hopping. For a half-filled system under periodic boundary conditions and $t_1 < t_2$ (topological regime), the system has a L scaling for the entanglement jump [see Fig. 12(c)] as was the case when $t_\perp = 0$ [see Fig. 10(a)]. Thus, for a periodic system, presence of a finite $t_\perp$ does not change the jump in the mutual entanglement. However, under open boundary conditions, the many-body ground state shows a $2\ln(2)$ entropy even at $\phi = 0$ and then jumps to a value of $(L+1)\ln(2)$ at $\phi > \pi/2$. This behavior seems to have an extra component of $2\ln(2)$ entropy added to the expected behavior of $(L-1)$ bulk unit cells which would contribute a entropy jump of $(L-1)\ln 2$ at $\phi = \frac{\pi}{2}$ [apart from the boundary sites the system has $L-1$ four site clusters, see Fig. 10(b)].

This extra entanglement can be understood from the fact that any interchain coupling immediately hybridizes the left (right) boundary mode of chain A with left (right) boundary mode of chain B with an energy $t_\perp$. This leads to a formation of two bonding like orbitals at the ends of our zigzag ladder (see Fig. 1) coupling the two chains A and B dominating over the physics of effective correlated hopping process whose energetics is exponentially small in system size [$\propto \alpha$, see Eq. (25)]. These boundary bonding orbitals adds a $2\ln(2)$ contribution of mutual entanglement entropy to the bulk part independent of ϕ. Thus, separating the bulk entanglement entropy part $\equiv S' = S - 2\ln(2)$, we can recover the expected scaling nature that is $\propto (L-1)\ln 2$ [see Fig. 12(d)].

Our discussion here, shows that—even though $t_\perp$ splits the boundary modes; perturbatively, the physics of the transition, entanglement jump between two phases and existence of the low-energy boundary sector under open boundary conditions remains stable when $t_\perp$ is smaller than the bulk gap. We have further checked that many-body polarization remains nontrivial in presence of $t_\perp$ (not shown).

VI. SUMMARY AND OUTLOOK

We now summarize our results. In this paper, using a combination of numerical and analytical calculations, we have shown that mutual statistics between quantum particles can be potentially "tuned" to engineer novel quantum mechanics for the low-energy subspaces formed out of topologically protected boundary modes in SPTs. We achieve, in particular, nontrivial tuning of the entanglement between the two one-dimensional chains which host topological phases using a statistical parameter ϕ. Our study therefore brings out an interesting interplay between quantum statistics, topological phases of matter, entanglement and symmetries.

As a concrete setting to achieve this end, we studied a system of pseudofermions on two distinct SSH chains. We noticed that for a half-filled system the boundary modes gets mutually entangled showing a jump in the entanglement entropy of $\ln(2)$ at $\phi = \frac{\pi}{2}$ (see Fig. 3). In Sec. IV, our study of just two particles in this system, provides a consistent understanding and the effective low-energy quantum mechanics of the boundary phenomena. Moving on to the bulk physics then, we found that ϕ engenders a first-order transition between two topological phases, again with a corresponding jump in the mutual entanglement entropy between the bulk sites (see Fig. 10). While such a transition is not specific to topological phases, here, it allows to entangle the boundary modes

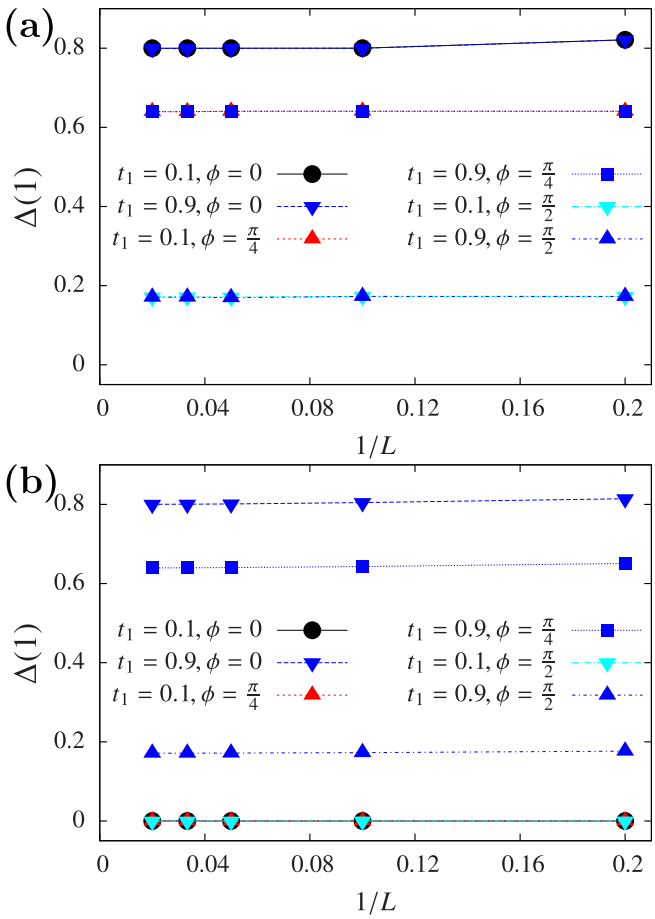

FIG. 13. Gap scaling. The scaling of energy gap to add one particle [$\Delta(1)$, see Eq. (36)] over the half-filled state with system size L for (a) periodic and (b) open boundary conditions for various values of t_1, $t_2 = 1 - t_1$, $\gamma = 2$, and ϕ. (DMRG results, further details in Appendix A).

nontrivially. We further investigated the role of disorder and various symmetry breaking and preserving perturbations to characterize the phase and its stability. Our work therefore points to an interesting class of phase and phase transitions, with potential technological implications, that can be engineered by tuning the algebra of these one-dimensional anyons. It might be interesting to compare the physics we discuss here with the physics of level crossings which occur in finite sized systems within a gapped topological phase due to presence of other perturbations [93–96]. While there, incommensurate correlations lead to level crossings between low lying eigenstates in the open system, these are not accompanied by a bulk first-order transition. Here on the other hand, the system undergoes a thermodynamic transition (which is independent of both system size and boundary conditions) at $\phi = \frac{\pi}{2}$. However, success in seeing their signatures in experiments [97], shows that similar protocols even in material systems can potentially allow for observation of a ϕ engineered first-order phase transition.

The possibility to tune the boundary modes and entangle them using statistical phase ϕ is particularly noteworthy given the exciting developments in the experimental forefront where the SSH model has been recently realized in a cold atomic setting—[46] using Rydberg atoms [98]. This experimental setting has shown unprecedented control in populating individual boundary modes and their possible manipulation and measurement [99]. The crucial ingredient of our system—i.e., the phase dependent correlated hopping has also been achieved experimentally [47], potentially making such manipulation of the boundary modes not very far from an actual experimental realization. These results, therefore, are of particular relevance in context of the study of the effective low-energy quantum mechanics of topological edge modes in one hand and their realization in ultracold atoms on the other. Devising concrete protocols for quantum gate operations in these low-energy subspaces could be an interesting future direction which would allow such platforms to be used for quantum computation. Finally, we conclude by re-emphasizing that our study points out that particle statistics is an interesting handle to uncover the rich interplay of entanglement, topological order and role of symmetries in quantum few and many-body phenomena.

ACKNOWLEDGMENTS

The authors acknowledge Gaurav K. Gupta and Vijay B. Shenoy for a previous collaboration. A.A. and S.B. acknowledge funding from Max Planck partner group grant at ICTS. S.B. acknowledges SERB-DST (India) for funding through project Grant No. ECR/2017/000504. Numerical calculations were performed on clusters *boson* at ICTS. We acknowledge use of open-source QUSPIN [100,101] and ITENSOR [102] for ED and DMRG calculations, respectively. We acknowledge the International Centre for Theoretical Sciences (ICTS) for supporting the program- Geometric phase in Optics and Topological Matter (Code: ICTS/geomtop2020/01) and the Department of Atomic Energy, Government of India, under Projects No. 12-R&D-TFR-5.10-1100 and No. RTI4001.

APPENDIX A: DMRG DETAILS AND GAP SCALING

Here in Fig. 13, we show the system size scaling of the energy gap $\Delta(1)$ [see Eq. (36)] which quantifies the amount of energy required to add one particle about the ground state at half-filling for both periodic and open system. In Fig. 10(d), we had seen its behavior as a function of ϕ for a particular system size. In Fig. 13, we show the scaling of this gap as a function of L showing that the single-particle gap remains finite even in the thermodynamic limit. Under open boundary conditions, this excitation energy goes to zero when $t_1 < t_2$ reflecting the existence of zero-energy boundary modes [see Fig. 13(b)].

We briefly mention the details of our DMRG calculations which were performed using open software ITENSOR [102]. ITENSOR uses a two-site DMRG update. Data pertaining to calculation of gap as shown in Figs. 10(c), 10(d) and 13 corresponds to evaluation of Eq. (36). Since the energy difference is being calculated for states belonging to different particle number sectors (which is a conserved quantity) one performs a ground-state DMRG for each particle number sector separately and then calculates the difference for calculating the excitation energy. In Fig. 13, 40 DMRG sweeps

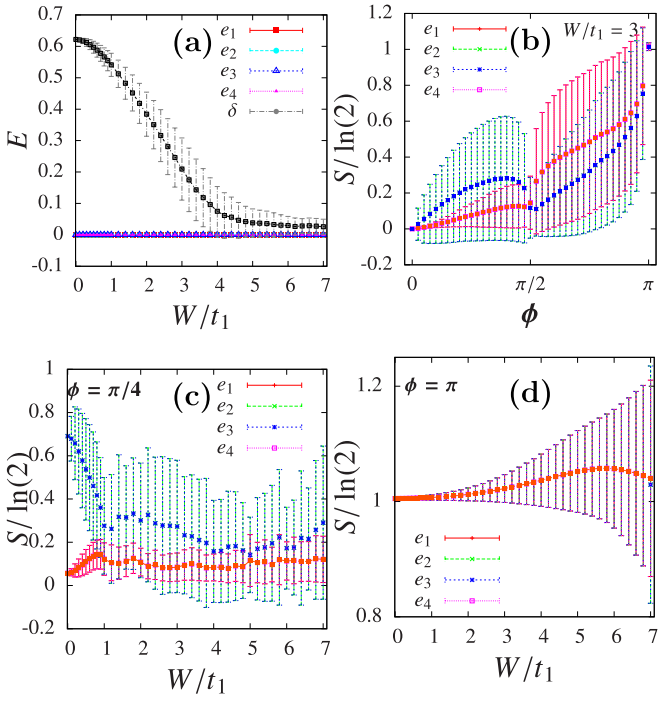

FIG. 14. Strong disorder. (a) Behavior of average energies of the four close to zero energy states [labeled $(e_1 - e_4)$] and the average energy gap to the bulk excited states defined as δ as a function of W/t_1 at $\phi = 0$. The averaging is done over 50 samples. The error bars reflect the standard deviation. (b) Entanglement entropies of the boundary modes as a function of ϕ for $W/t_1 = 3$. [(c) and (d)] The entanglement entropies of the boundary modes as a function of W/t_1 in (c) $\phi = \pi/4$ and (d) $\phi = \pi$. (ED, $N = 4L = 40$, $t_1 = 0.1 = 1 - t_2$, and $\gamma = 2$).

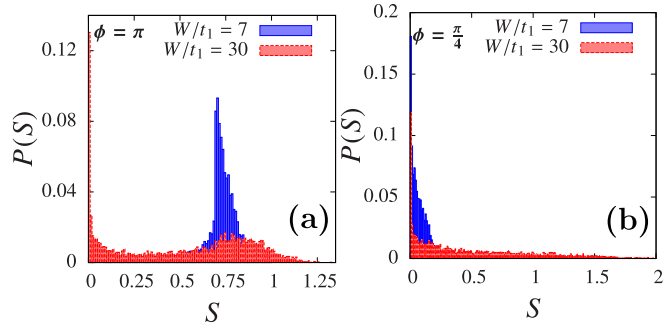

FIG. 15. Probability distribution of S. The probability distribution of the mutual entanglement entropy $P(S)$ for the two-particle boundary mode (e_1) for different values of hopping disorder strength W/t_1 in (a) for $\phi = \pi$ and $W/t_1 = 7, 30$ and in (b) for $\phi = \pi/4$ and $W/t_1 = 7, 30$. The distribution at large W/t_1 is not a normal distribution. The sampling is done for 5000 independent disorder configurations. (ED, $t_1 = 0.1$, $t_2 = 1 - t_1$, $\gamma = 2$, $N = 4L = 40$, and bin size $= 0.01$).

were performed where the bond dimension was systematically increased up to a value of 200. The truncation error is kept at 10^{-10} and after 40 sweeps typically the energies would converge up to a precision of 10^{-8}. In Figs. 10(c) and 10(d), we instead use 10 sweeps.

APPENDIX B: DISORDER AVERAGING

In Fig. 7, we had shown the entanglement entropy of the boundary modes as a function of ϕ in presence of hopping disorder of strength W. Here, we systematically increase the value of W and analyze the behavior of entanglement entropies in Fig. 14. Given the presence of one particle on each chain; in Fig. 14(a), we compare the energies of the near-zero energy modes and the gap to the bulk-excited states ($\equiv \delta$) at $\phi = 0$. We find that the band-gap collapses near $W/t_1 \sim 3$ for $t_1 = 0.1 = 1 - t_2$, $\gamma = 2$. We investigate the entanglement entropy as a function of W/t_1 for various values of ϕ in Figs. 14(c) and 14(d). While for low values of $W (\ll \delta)$ the fluctuations in the entanglement entropy remains small, but with large W these fluctuations become significantly large. Investigating the probability distribution of S (see Fig. 15), we find that at large W/t_1, S is far from any normal distribution consistent with studies of entanglement entropy in strongly disordered systems [87,88]. It is useful to note entanglement entropy can be consistently defined only for nondegenerate eigenstates, therefore in sample averaging we discard states which are degenerate up to machine precision ($\sim 10^{-14}$).

We briefly mention here the details of the ED calculation which were performed using QUSPIN [100,101]. ED calculations, both in absence/presence of disorder, were performed on finite sized systems without any symmetry implementation. For systems at half filling, when we were interested only in low-energy eigenvalues and wave functions, standard PYTHON based sparse solvers were used that are declared within the QUSPIN package.

[1] X.-G. Wen, Rev. Mod. Phys. **89**, 041004 (2017).
[2] A. W. W. Ludwig, Phys. Scr. **2016**, 014001 (2016).
[3] C.-K. Chiu, J. C. Y. Teo, A. P. Schnyder, and S. Ryu, Rev. Mod. Phys. **88**, 035005 (2016).
[4] M. Z. Hasan and C. L. Kane, Rev. Mod. Phys. **82**, 3045 (2010).
[5] X.-L. Qi and S.-C. Zhang, Rev. Mod. Phys. **83**, 1057 (2011).
[6] Y. Ando, J. Phys. Soc. Jpn. **82**, 102001 (2013).
[7] K. Yang, W. Setyawan, S. Wang, M. Buongiorno Nardelli, and S. Curtarolo, Nat. Mater. **11**, 614 (2012).
[8] C. Beenakker, Annu. Rev. Condens. Matter Phys. **4**, 113 (2013).
[9] M. G. Vergniory, L. Elcoro, C. Felser, N. Regnault, B. A. Bernevig, and Z. Wang, Nature **566**, 480 (2019).
[10] J. Kruthoff, J. de Boer, J. van Wezel, C. L. Kane, and R.-J. Slager, Phys. Rev. X **7**, 041069 (2017).
[11] R.-J. Slager, A. Mesaros, V. Juričić, and J. Zaanen, Nat. Phys. **9**, 98 (2013).
[12] W. P. Su, J. R. Schrieffer, and A. J. Heeger, Phys. Rev. B **22**, 2099 (1980).

[13] W. P. Su, J. R. Schrieffer, and A. J. Heeger, Phys. Rev. Lett. **42**, 1698 (1979).
[14] A. Y. Kitaev, Phys. Usp. **44**, 131 (2001).
[15] J. Alicea, Rep. Prog. Phys. **75**, 076501 (2012).
[16] V. Mourik, K. Zuo, S. M. Frolov, S. Plissard, E. P. Bakkers, and L. P. Kouwenhoven, Science **336**, 1003 (2012).
[17] A. Das, Y. Ronen, Y. Most, Y. Oreg, M. Heiblum, and H. Shtrikman, Nat. Phys. **8**, 887 (2012).
[18] C. Nayak, S. H. Simon, A. Stern, M. Freedman, and S. Das Sarma, Rev. Mod. Phys. **80**, 1083 (2008).
[19] T. Hyart, B. van Heck, I. C. Fulga, M. Burrello, A. R. Akhmerov, and C. W. J. Beenakker, Phys. Rev. B **88**, 035121 (2013).
[20] D. Aasen, M. Hell, R. V. Mishmash, A. Higginbotham, J. Danon, M. Leijnse, T. S. Jespersen, J. A. Folk, C. M. Marcus, K. Flensberg, and J. Alicea, Phys. Rev. X **6**, 031016 (2016).
[21] P. Boross, J. K. Asbóth, G. Széchenyi, L. Oroszlány, and A. Pályi, Phys. Rev. B **100**, 045414 (2019).
[22] M. Zaimi, C. Boudreault, N. Baspin, H. Eleuch, R. MacKenzie, and M. Hilke, Qubits as edge state detectors: illustration using the ssh model, arXiv:1910.12739 [cond-mat.mes-hall].
[23] F. Mei, G. Chen, L. Tian, S.-L. Zhu, and S. Jia, Phys. Rev. A **98**, 032323 (2018).
[24] D. Baeriswyl and K. Maki, Phys. Rev. B **28**, 2068 (1983).
[25] K. Padavić, S. S. Hegde, W. DeGottardi, and S. Vishveshwara, Phys. Rev. B **98**, 024205 (2018).
[26] S.-L. Zhang and Q. Zhou, Phys. Rev. A **95**, 061601(R) (2017).
[27] A. A. Nersesyan, Phys. Rev. B **102**, 045108 (2020).
[28] G. Ghelli, G. Magnifico, C. D. E. Boschi, and E. Ercolessi, Phys. Rev. B **101**, 085124 (2020).
[29] F. Harper, A. Pushp, and R. Roy, Phys. Rev. Res. **1**, 033207 (2019).
[30] S. Longhi, Phys. Rev. B **99**, 155150 (2019).
[31] N. Lang and H. P. Büchler, npj Quantum Inf. **3**, 47 (2017).
[32] T. D. Stanescu and S. Tewari, J. Phys.: Cond. Matter **25**, 233201 (2013).
[33] S. Nadj-Perge, I. K. Drozdov, J. Li, H. Chen, S. Jeon, J. Seo, A. H. MacDonald, B. A. Bernevig, and A. Yazdani, Science **346**, 602 (2014).
[34] L. P. Rokhinson, X. Liu, and J. K. Furdyna, Nat. Phys. **8**, 795 (2012).
[35] E. Dumitrescu, B. Roberts, S. Tewari, J. D. Sau, and S. Das Sarma, Phys. Rev. B **91**, 094505 (2015).
[36] M. T. Deng, S. Vaitiekėnas, E. B. Hansen, J. Danon, M. Leijnse, K. Flensberg, J. Nygård, P. Krogstrup, and C. M. Marcus, Science **354**, 1557 (2016).
[37] S. M. Albrecht, A. P. Higginbotham, M. Madsen, F. Kuemmeth, T. S. Jespersen, J. Nygård, P. Krogstrup, and C. Marcus, Nature (London) **531**, 206 (2016).
[38] M. Deng, C. Yu, G. Huang, M. Larsson, P. Caroff, and H. Xu, Nano Lett. **12**, 6414 (2012).
[39] J. Liu, A. C. Potter, K. T. Law, and P. A. Lee, Phys. Rev. Lett. **109**, 267002 (2012).
[40] J. Klinovaja, P. Stano, A. Yazdani, and D. Loss, Phys. Rev. Lett. **111**, 186805 (2013).
[41] R. M. Lutchyn, E. P. Bakkers, L. P. Kouwenhoven, P. Krogstrup, C. M. Marcus, and Y. Oreg, Nat. Rev. Mater. **3**, 52 (2018).
[42] X. Li, E. Zhao, and W. V. Liu, Nat. Commun. **4**, 1523 (2013).
[43] E. J. Meier, F. A. An, and B. Gadway, Nat. Commun. **7**, 13986 (2016).
[44] M. Leder, C. Grossert, L. Sitta, M. Genske, A. Rosch, and M. Weitz, Nat. Commun. **7**, 13112 (2016).
[45] D. Xie, W. Gou, T. Xiao, B. Gadway, and B. Yan, npj Quantum Inf. **5**, 55 (2019).
[46] S. de Léséleuc, V. Lienhard, P. Scholl, D. Barredo, S. Weber, N. Lang, H. P. Büchler, T. Lahaye, and A. Browaeys, Science **365**, 775 (2019).
[47] V. Lienhard, P. Scholl, S. Weber, D. Barredo, S. de Léséleuc, R. Bai, N. Lang, M. Fleischhauer, H. P. Büchler, T. Lahaye, and A. Browaeys, Phys. Rev. X **10**, 021031 (2020).
[48] Z.-W. Zuo, G.-L. Li, and L. Li, Phys. Rev. B **97**, 115126 (2018).
[49] S. Greschner, L. Cardarelli, and L. Santos, Phys. Rev. A **97**, 053605 (2018).
[50] A. Agarwala, G. K. Gupta, V. B. Shenoy, and S. Bhattacharjee, Phys. Rev. B **99**, 165125 (2019).
[51] J. M. Leinaas and J. Myrheim, Il Nuovo Cimento B (1971-1996) **37**, 1 (1977).
[52] E. H. Lieb and W. Liniger, Phys. Rev. **130**, 1605 (1963).
[53] A. Kundu, Phys. Rev. Lett. **83**, 1275 (1999).
[54] V. Pasquier, *Integrable Models and Strings*, edited by A. Alekseev, A.Heitamäki, K. Huitu, A. Morozov, and A. Niemi (Springer, Berlin, Heidelberg, 1994), pp. 36–48.
[55] Z. N. C. Ha, Phys. Rev. Lett. **73**, 1574 (1994).
[56] Z. Ha, Nucl. Phys. B **435**, 604 (1995).
[57] C. Aneziris, A. P. Balachandran, and D. Sen, Int. J. Mod. Phys. A **6**, 4721 (1991).
[58] T. Posske, B. Trauzettel, and M. Thorwart, Phys. Rev. B **96**, 195422 (2017).
[59] M. Frau, A. Lerda, and S. Sciuto, in *Proceedings of the CXXVII International School of Physics "E. Fermi" on "Quantum Groups and their Applications in Physics"* (IOS Press, Amsterdam, 1996), Vol. 215.
[60] M. El Baz and Y. Hassouni, Int. J. Mod. Phys. A **18**, 3015 (2003).
[61] F. D. M. Haldane, Phys. Rev. Lett. **67**, 937 (1991).
[62] Y.-S. Wu, Phys. Rev. Lett. **73**, 922 (1994).
[63] M. V. N. Murthy and R. Shankar, Phys. Rev. Lett. **73**, 3331 (1994).
[64] M. T. Batchelor, X.-W. Guan, and N. Oelkers, Phys. Rev. Lett. **96**, 210402 (2006).
[65] H. Guo, Y. Hao, and S. Chen, Phys. Rev. A **80**, 052332 (2009).
[66] M. Eckholt and J. J. García-Ripoll, New J. Phys. **11**, 093028 (2009).
[67] M. Eckholt and J. J. García-Ripoll, Phys. Rev. A **77**, 063603 (2008).
[68] S. Greschner and L. Santos, Phys. Rev. Lett. **115**, 053002 (2015).
[69] J. Arcila-Forero, R. Franco, and J. Silva-Valencia, Phys. Rev. A **94**, 013611 (2016).
[70] W. Zhang, S. Greschner, E. Fan, T. C. Scott, and Y. Zhang, Phys. Rev. A **95**, 053614 (2017).
[71] F. Lange, S. Ejima, and H. Fehske, Phys. Rev. Lett. **118**, 120401 (2017).

[72] F. Lange, S. Ejima, and H. Fehske, Phys. Rev. A **95**, 063621 (2017).
[73] J. Arcila-Forero, R. Franco, and J. Silva-Valencia, Phys. Rev. A **97**, 023631 (2018).
[74] S. S. Pershoguba and V. M. Yakovenko, Phys. Rev. B **86**, 075304 (2012).
[75] B. N. Narozhny and A. Levchenko, Rev. Mod. Phys. **88**, 025003 (2016).
[76] K. Lee, J. Xue, D. C. Dillen, K. Watanabe, T. Taniguchi, and E. Tutuc, Phys. Rev. Lett. **117**, 046803 (2016).
[77] J. I. A. Li, T. Taniguchi, K. Watanabe, J. Hone, A. Levchenko, and C. R. Dean, Phys. Rev. Lett. **117**, 046802 (2016).
[78] A. Altland and M. R. Zirnbauer, Phys. Rev. B **55**, 1142 (1997).
[79] A. Agarwala, A. Haldar, and V. B. Shenoy, Ann. Phys. **385**, 469 (2017).
[80] S. Ryu, A. P. Schnyder, A. Furusaki, and A. W. W. Ludwig, New J. Phys. **12**, 065010 (2010).
[81] A. Kitaev, *Advances in Theoretical Physics: Landau Memorial Conference*, edited by V. Lebedev and M. Feigel'man, AIP Conf. Proc. 1134 (AIP, Melville, NY, 2009), pp. 22–30.
[82] J. Eisert, M. Cramer, and M. B. Plenio, Rev. Mod. Phys. **82**, 277 (2010).
[83] L. Amico, R. Fazio, A. Osterloh, and V. Vedral, Rev. Mod. Phys. **80**, 517 (2008).
[84] J. K. Asbóth, L. Oroszlány, and A. Pályi, Lect. Notes Phys. **919**, 997 (2016).
[85] D. A. Abanin and E. Demler, Phys. Rev. Lett. **109**, 020504 (2012).
[86] P. W. Anderson, Phys. Rev. **109**, 1492 (1958).
[87] N. Laflorencie, Phys. Rev. B **72**, 140408(R) (2005).
[88] L. Pastur and V. Slavin, J. Stat. Phys. **170**, 207 (2018).
[89] R. D. King-Smith and D. Vanderbilt, Phys. Rev. B **47**, 1651 (1993).
[90] R. Resta and D. Vanderbilt, *Physics of Ferroelectrics* (Springer, Berlin, 2007), pp. 31–68.
[91] M. Nakamura and J. Voit, Phys. Rev. B **65**, 153110 (2002).
[92] H. Watanabe and M. Oshikawa, Phys. Rev. X **8**, 021065 (2018).
[93] F. Mila, Nat. Phys. **12**, 633 (2016).
[94] G. Vionnet, B. Kumar, and F. Mila, Phys. Rev. B **95**, 174404 (2017).
[95] N. Chepiga and F. Mila, Phys. Rev. B **96**, 060409(R) (2017).
[96] N. Chepiga and F. Mila, Phys. Rev. B **97**, 174434 (2018).
[97] R. Toskovic, R. van den Berg, A. Spinelli, I. Eliens, B. van den Toorn, B. Bryant, J.-S. Caux, and A. Otte, Nat. Phys. **12**, 656 (2016).
[98] A. Browaeys and T. Lahaye, Nat. Phys. **16**, 132 (2020).
[99] A. Elben, J. Yu, G. Zhu, M. Hafezi, F. Pollmann, P. Zoller, and B. Vermersch, Sci. Adv. **6**, eaaz3666 (2020).
[100] P. Weinberg and M. Bukov, SciPost Phys. **2**, 003 (2017).
[101] P. Weinberg and M. Bukov, SciPost Phys. **7**, 20 (2019).
[102] ITensor, http://itensor.org/.